

Supporting information

**Intermolecular  $\pi$ -stacking stabilization of new coordination motif with amplified M/L ratio for dinuclear Fe(III) complex supported by “salen type” Schiff base derivative of o-xylylenediamine**

Ilia D. Shutilov<sup>a</sup>, Pavel A. Volodin<sup>b</sup>, Alexander S. Ovsyannikov<sup>a\*</sup>, Andrew V. Pyataev<sup>b</sup>, Lubov V. Frantsuzova<sup>a</sup>, Daria P. Gerasimova<sup>a</sup>, Ayrat R. Khamatgalimov<sup>a</sup>, Svetlana E. Solovieva<sup>a</sup>, Igor S. Antipin<sup>b</sup>

<sup>a</sup>*A. E. Arbuzov Institute of Organic and Physical Chemistry, FRC Kazan Scientific Center, Russian Academy of Sciences, Arbuzova 8 str., 420088 Kazan, Russian Federation*

<sup>b</sup>*Kazan Federal University, Kremlevskaya 18 str., 420008 Kazan, Russian Federation*

\*Corresponding author: osaalex2007@rambler.ru

## 1. Experimental section

All chemicals were purchased from commercial suppliers and used without additional purification. Solvents were purified according to standard procedures.<sup>1</sup>

<sup>1</sup>H/<sup>13</sup>C NMR spectra were recorded on AVANCE II<sup>TM</sup> 600/151MHz BRUKER BioSpin (Germany) with signals from residual protons of CDCl<sub>3</sub> as internal standard.

The MALDI mass spectra were recorded on an Ultraflex III TOF/TOF mass spectrometer (Bruker Daltonic GmbH, Bremen, Germany) operated in the linear mode with the registration of positively charged ions. 2,5-Dihydroxybenzoic acid (DHB) was used as a matrix.

Infrared spectra (IR) of milled crystalline samples in KBr were recorded on a Tensor 27 Fourier-transform spectrometer (Bruker) in a range of 4000-400 cm<sup>-1</sup> with an optical resolution of 4 cm<sup>-1</sup> and an accumulation of 32 scans.

The powder X-ray diffraction (PXRD) patterns for **2-Dy** complex were measured using an X-ray powder diffractometer (DX-2700BH, Haoyuan, China), with a Cu-radiation,  $\text{K}\alpha = 1.5418 \text{ \AA}$ , at 40 kV and 30 mA. The data were collected in the reflection mode with a flat plate sample at room temperature. Sample was applied on the surface of a standard zero diffraction silicon plate, which reduces background scattering. The PXRD patterns were recorded in the  $2\theta$  range between 3° and 40° with 0.02° step and 0.1 sec exposition time. Several diffraction patterns were obtained sequentially for the sample during the solvate molecules release processus and until the observed solid phase transformation was completed.

A TGA/DSC NETZSCH (Selb, Germany) STA449 F3 were used for the thermal analysis (thermogravimetry/differential scanning calorimetry) in which the variation of the sample mass as a function of temperature and the corresponding heats are recorded. An approximately 15 mg sample was placed in an Al crucible with a pre-hole on the lid and heated from 25 to 500°C. The same empty crucible was used as the reference sample. High-purity argon was used with a gas flow rate of 50mL/min. TGA measurement were performed at the heating rates of 5 K/min

Elemental analysis was performed on a EuroEA 3028-HT-OM Eurovector S.p.A. (Italy).

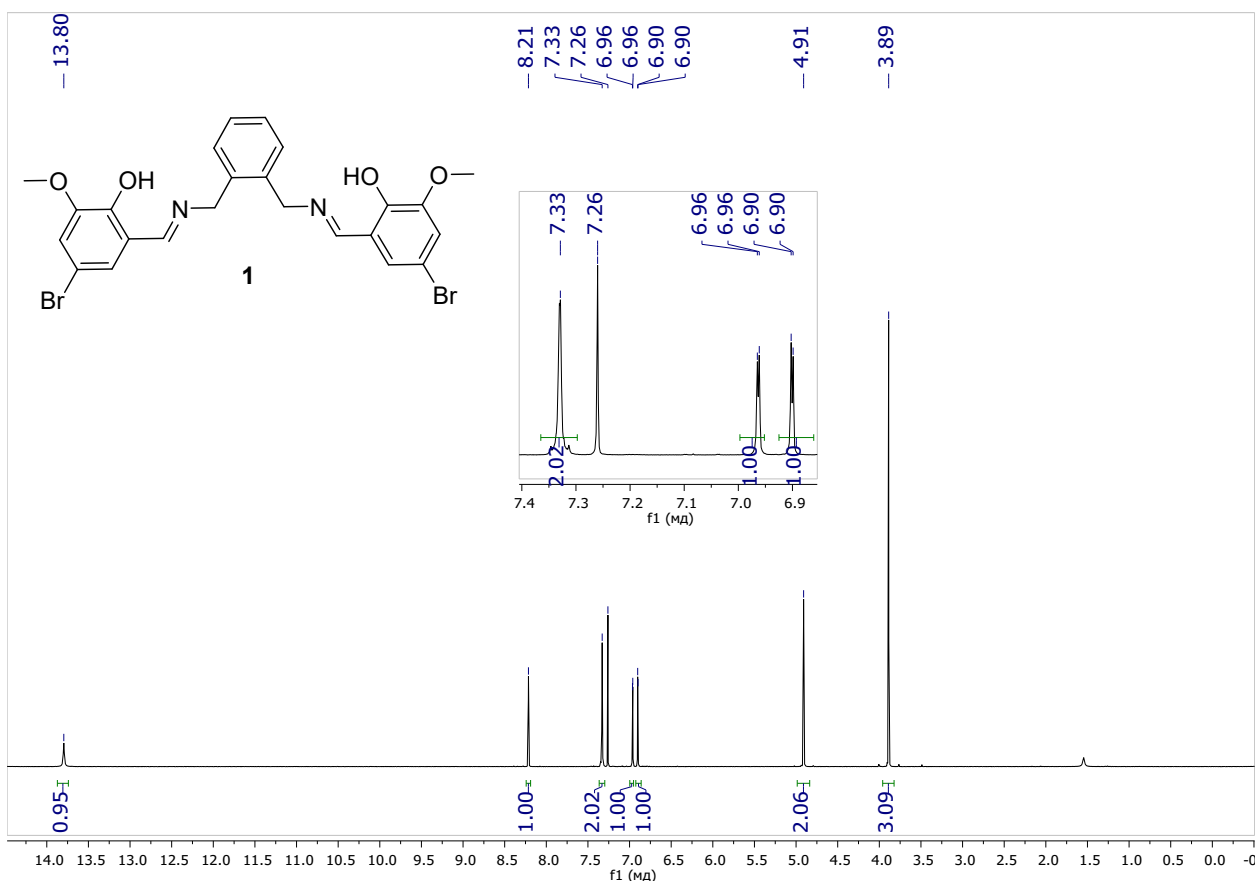
## 2. Synthesis of ligands 1-3

**1:** 5-bromo-2-hydroxy-3-methoxybenzaldehyde (0.534 g, 2.31 mmol) was added to a solution of *o*-xylylene dibromide (0.150 g, 1.10 mmol) in methanol (20 ml), and the reaction mixture was stirred at room temperature for 5 h. The yellow precipitate was formed, then filtered off, washed with cold methanol (10 ml) and dried under vacuum at room temperature, affording a pure product (0.483 g, 78%).  $M_p = 177.12\text{ }^\circ\text{C}$ .  $^1\text{H}$  NMR (600 MHz,  $\text{CDCl}_3$ )  $\delta$ , ppm: 3.89 (6H, s,  $\text{CH}_3$ ), 4.91 (4H, s,  $\text{CH}_2$ ), 6.90 (2H, d,  $^4J=1.8$   $\text{CH}_{\text{Ar}}$ ), 6.96 (2H, d,  $^4J=2.4$   $\text{CH}_{\text{Ar}}$ ), 7.31-7.35 (4H, m,  $\text{CH}_{\text{Ar}}$ ), 8.21 (2H, s,  $\text{CH}=\text{N}$ ), 13.80 (2H, s, OH).  $^{13}\text{C}$  NMR (151 MHz,  $\text{CDCl}_3$ )  $\delta$ , ppm: 56.48, 60.01, 109.56, 117.36, 119.36, 125.01, 128.63, 129.74, 135.60, 149.50, 151.15, 165.12. MALDI-MS, m/z: 563.2 [ $\text{M}+\text{H}]^+$  ( $m/z_{\text{calc}} = 563.0$ ), 585.2 [ $\text{M}+\text{Na}]^+$  ( $m/z_{\text{calc}} = 584.9$ ), 601.2 [ $\text{M}+\text{K}]^+$  ( $m/z_{\text{calc}} = 600.9$ ). IR (KBr,  $\text{cm}^{-1}$ )  $\nu$ : 3440(m), 3081(w), 3014(w), 2963(w), 2935(w), 2898(w), 2835(w), 1632(s), 1573 (m) 1470(s), 1396(m), 1375(m), 1333(m), 1321(m), 1270(s), 1252(s), 1185(w), 1149(w), 1096(m), 1054(m), 1028(m), 976(m), 953(m), 865(m), 844(m), 769(m), 697(w), 576(w). Anal. calcd for  $\text{C}_{24}\text{H}_{22}\text{Br}_2\text{N}_2\text{O}_4$ , %: C, 51.27; H, 3.94; N, 4.98. Found, %: C, 51.21; H, 3.96; N, 5.03.

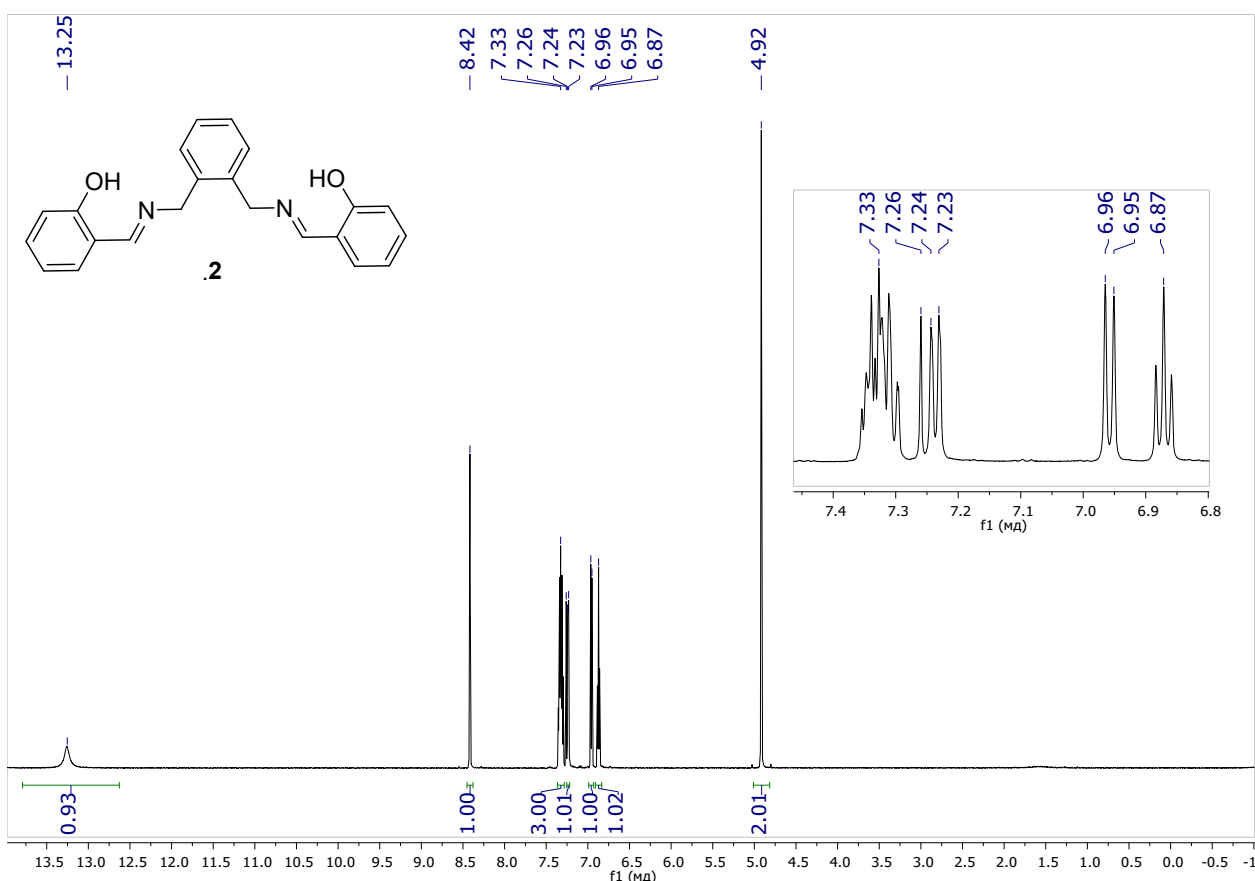
**2:** 2-Hydroxy-benzaldehyde (0.454 g, 3.72 mmol) was added to a solution of *o*-xylylene dibromide (0.230 g, 1.69 mmol) in methanol (20 ml), and the reaction mixture was stirred at room temperature for 5 h. The yellow precipitate was formed, then filtered off, washed with cold methanol (10 ml) and dried under vacuum at room temperature, affording a pure product (0.483 g, 83%).  $M_p = 98.0\text{ }^\circ\text{C}$ .  $^1\text{H}$  NMR (600 MHz,  $\text{CDCl}_3$ )  $\delta$ , ppm: 4.92 (4H, s,  $\text{CH}_2$ ), 6.87 (2H, t,  $^3J=7.2$  Hz,  $\text{CH}_{\text{Ar}}$ ), 6.95 (2H, d,  $^3J=8.4$  Hz,  $\text{CH}_{\text{Ar}}$ ), 7.24 (2H, d,  $^3J=7.8$  Hz,  $\text{CH}_{\text{Ar}}$ ), 7.29-7.36 (6H, m,  $\text{CH}_{\text{Ar}}$ ), 8.42 (2H, s,  $\text{CH}=\text{N}$ ), 13.25 (2H, s, OH).  $^{13}\text{C}$  NMR (151 MHz,  $\text{CDCl}_3$ )  $\delta$ , ppm: 60.61, 117.14, 118.86, 118.96, 128.24, 129.29, 131.66, 132.62, 136.14, 161.12, 166.16. MALDI-MS, m/z: 345.1 [ $\text{M}+\text{H}]^+$  ( $m/z_{\text{calc}} = 344.2$ ), 367.1 [ $\text{M}+\text{Na}]^+$  ( $m/z_{\text{calc}} = 364.1$ ). IR (KBr,  $\text{cm}^{-1}$ )  $\nu$ : 3050(m), 3011(m), 2922(m), 2891(m), 2869(m), 2728(m), 2633(m), 1673(w), 1629(s), 1578(s), 1530(w), 1496(s), 1460(s), 1428(m), 1405(m), 1374(m), 1343(w), 1328(w), 1316(w), 1279(s), 1205(m), 1153(m), 1116(m), 1060(m), 1034(m), 1000(m), 979(m), 944(w), 759(m), 657(m). Anal. calcd for  $\text{C}_{22}\text{H}_{20}\text{N}_2\text{O}_2$ , %: C, 76.72; H, 5.85; N, 8.13. Found, %: C, 76.75; H, 5.82; N, 8.16.

**3:** 2-Hydroxy-3-methoxybenzaldehyde (0.804 g, 5.29 mmol) was added to a solution of *o*-xylinedibromide (0.360 g, 2.64 mmol) in methanol (50 ml), and the rection mixture was stirred at room temperature for 5 h. The yellow precipitate was formed, filtered off, washed with cold methanol (10 ml) affording a pure product (0.812 g, 76%).  $M_p = 113.3\text{ }^\circ\text{C}$ .  $^1\text{H}$  NMR (600 MHz,  $\text{CDCl}_3$ )  $\delta$ , ppm: 3.89 (6H, s,  $\text{CH}_3$ ), 4.91 (4H, s,  $\text{CH}_2$ ), 6.80 (2H, t,  $^2J=7.8$  Hz,  $\text{CH}_{\text{Ar}}$ ), 6.87 (2H, dd,  $^3J=7.8$  Hz,  $^4J=1.3$  Hz,  $\text{CH}_{\text{Ar}}$ ), 6.92 (2H, dd,  $^3J=8.4$  Hz,  $^4J=1.2$  Hz,  $\text{CH}_{\text{Ar}}$ ), 7.27-7.30 (2H, m,  $\text{CH}_{\text{Ar}}$ ), 7.31-7.35 (2H, m,  $\text{CH}_{\text{Ar}}$ ), 8.41 (2H, s,  $\text{CH}=\text{N}$ ), 13.76 (2H, s, OH).  $^{13}\text{C}$  NMR (151 MHz,  $\text{CDCl}_3$ )  $\delta$ , ppm: 56.22, 60.33, 114.37, 118.22, 118.77, 123.23, 128.14, 129.00, 135.97, 148.49, 151.57, 166.20. MALDI-MS, m/z: 405.1 [ $\text{M}+\text{H}]^+$  ( $m/z_{\text{calc}} = 405.2$ ). IR (KBr,  $\text{cm}^{-1}$ )  $\nu$ : 3448(m), 1628(s), 1472(s), 1429(m), 1377(w), 1335(w), 1170(w), 1077(m), 1055(m), 1018(m), 955(m), 839(w), 769(m), 735 (m). Anal. calcd for  $\text{C}_{24}\text{H}_{24}\text{N}_2\text{O}_4$ , %: C, 71.27; H, 5.98; N, 6.93. Found, %: C, 71.31; H, 5.95; N, 6.98

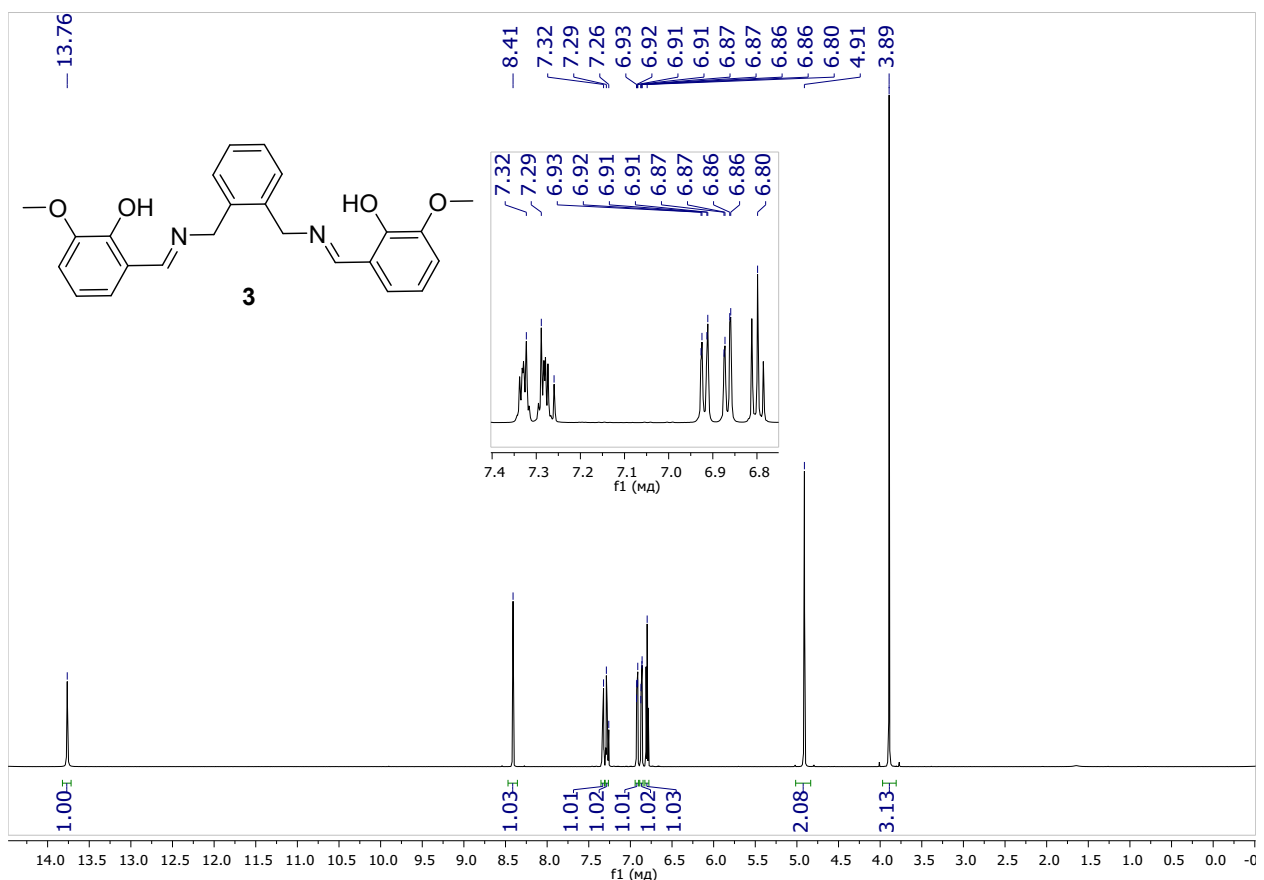
### 3. Characterization of ligands



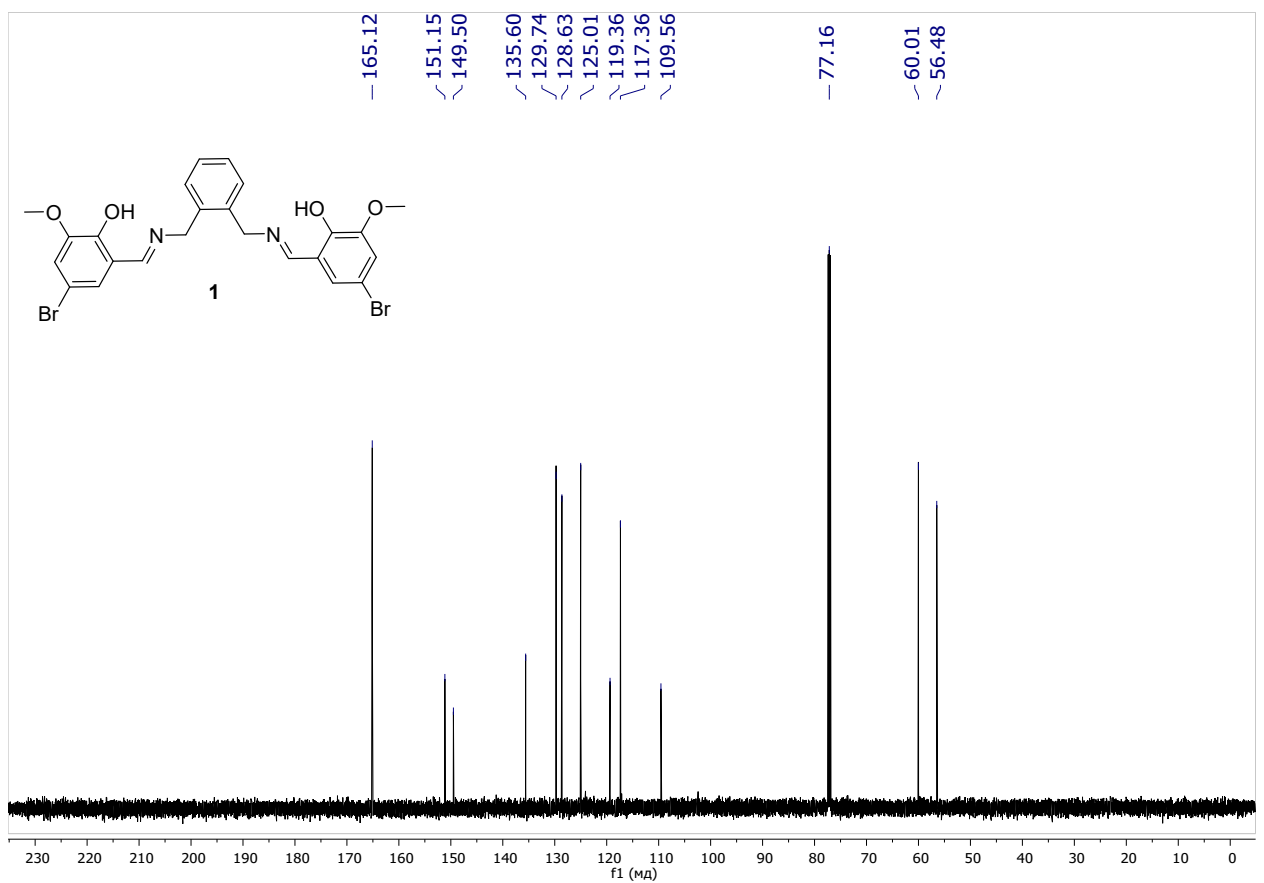
**Figure S1.**  $^1\text{H}$  NMR spectrum for **1** ( $\text{CDCl}_3$ , 600 MHz, 25 °C).



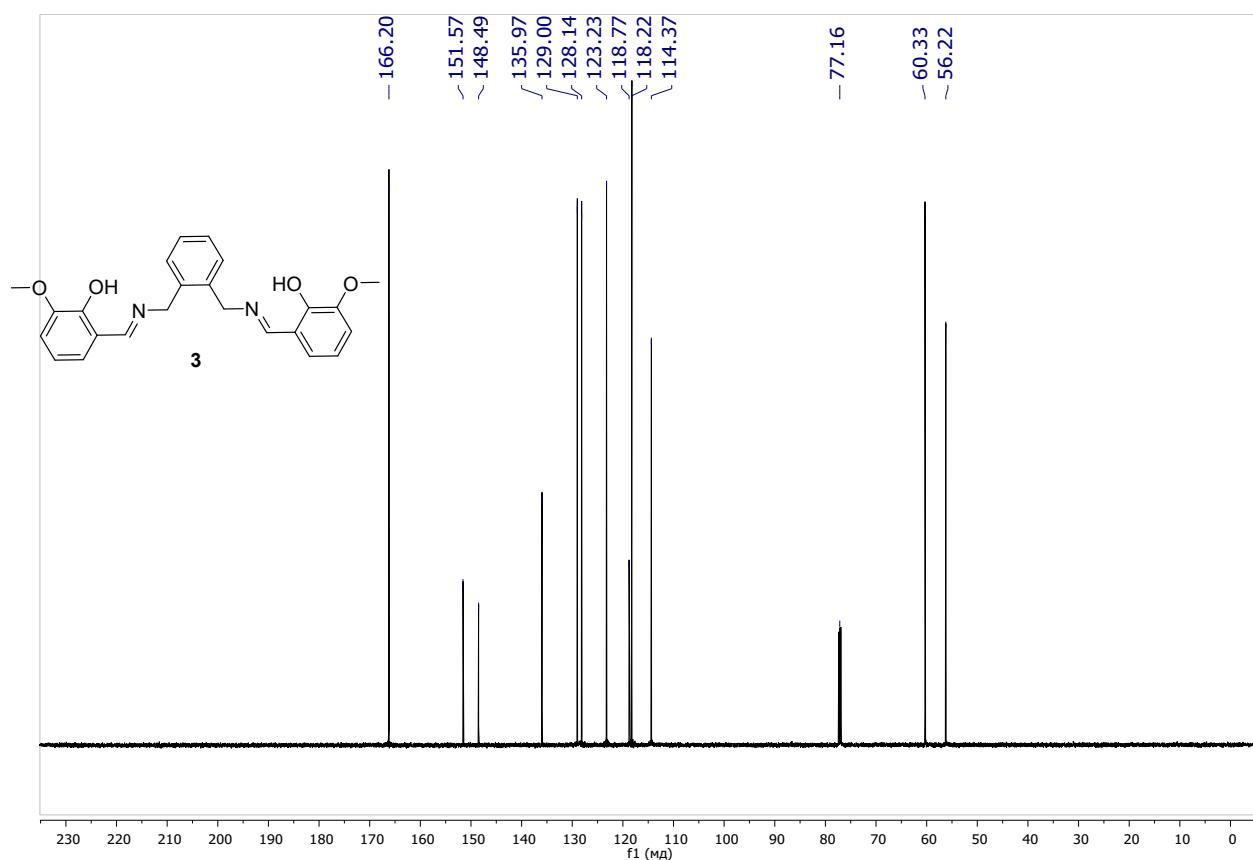
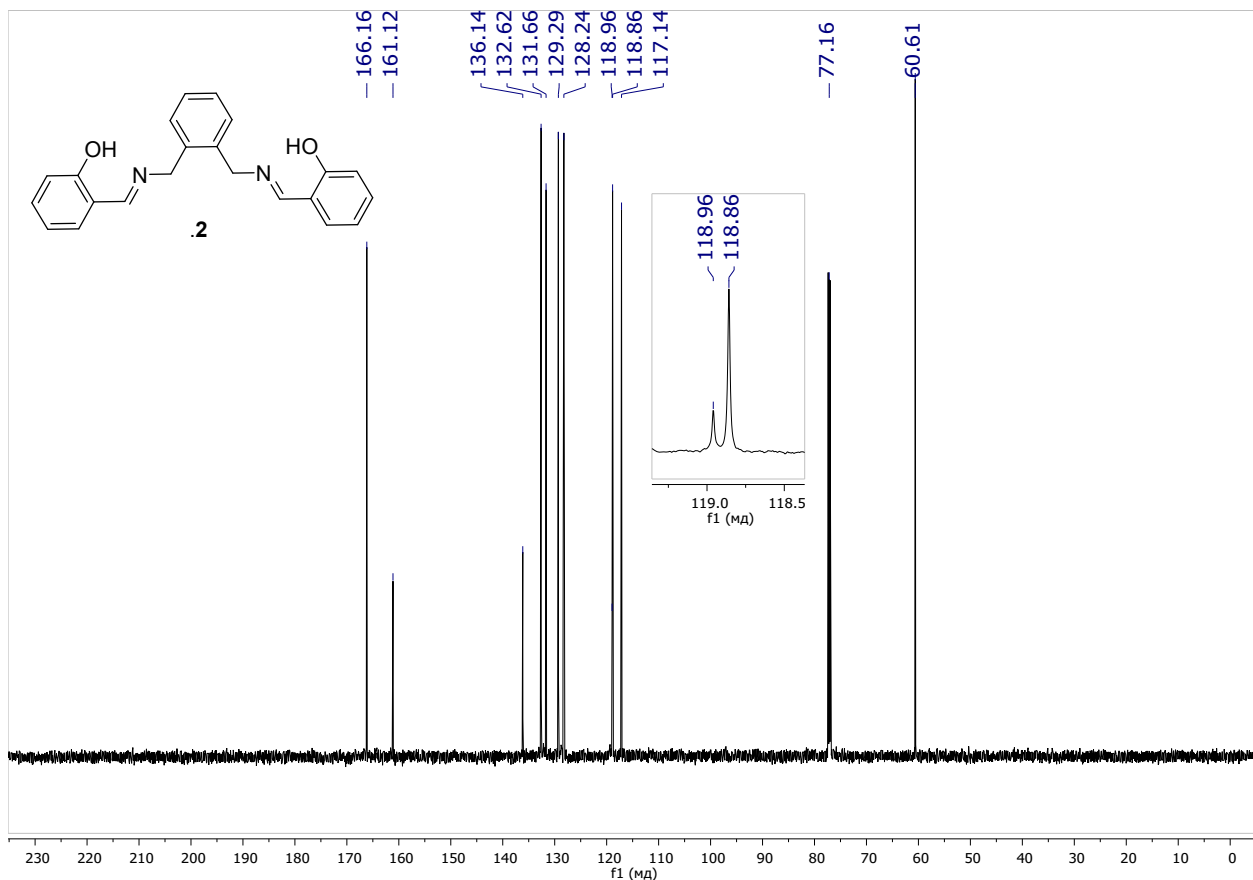
**Figure S2.**  $^1\text{H}$  NMR spectrum for **2** ( $\text{CDCl}_3$ , 600 MHz, 25 °C).



**Figure S3.**  $^1\text{H}$  NMR spectrum for **3** ( $\text{CDCl}_3$ , 600 MHz, 25 °C).



**Figure S4.**  $^{13}\text{C}$  NMR spectrum for **1** ( $\text{CDCl}_3$ , 151 MHz, 25 °C).



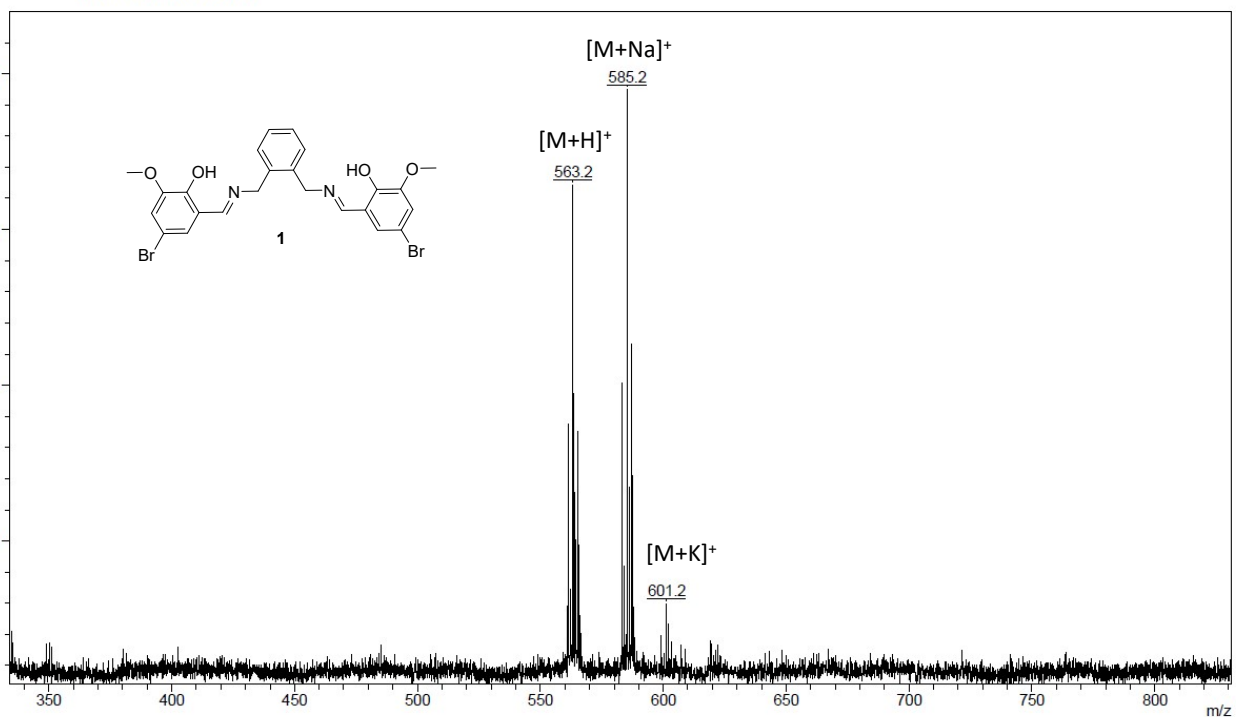


**Figure S7.** MALDI-MS spectrum for **1**.

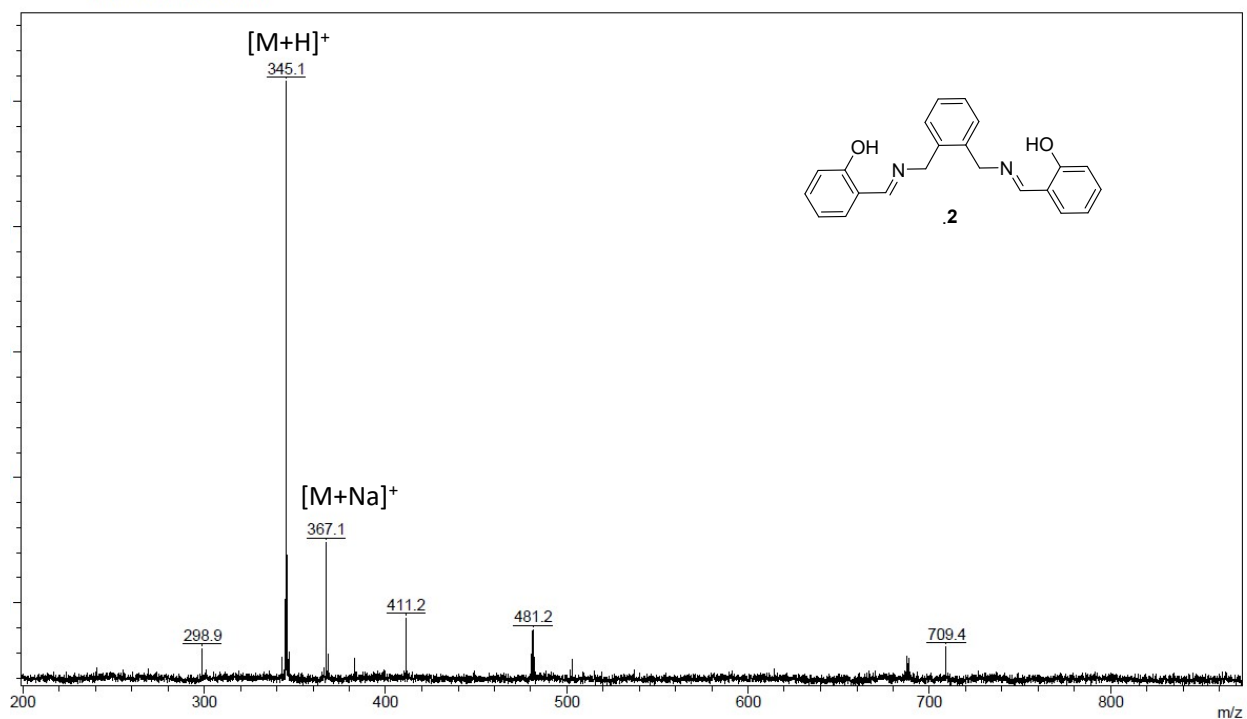


**Figure S8.** MALDI-MS spectrum for **2**.

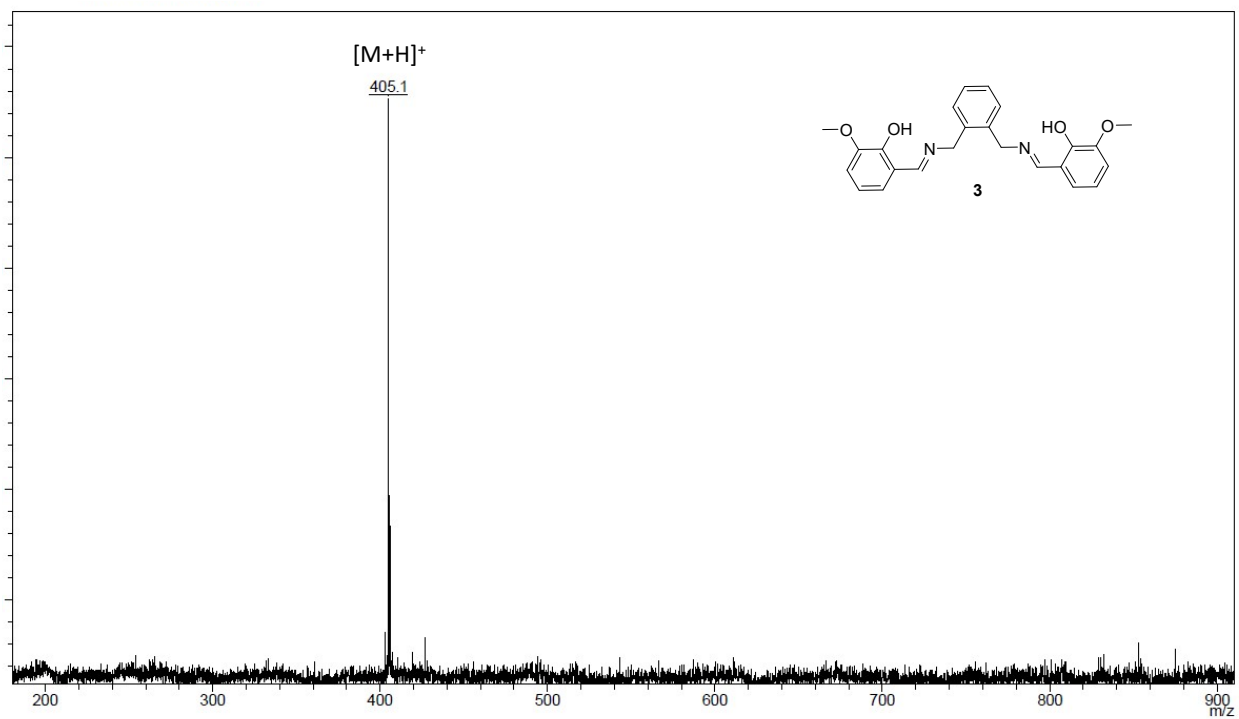


**Figure S9.** MALDI-MS spectrum for **3**.

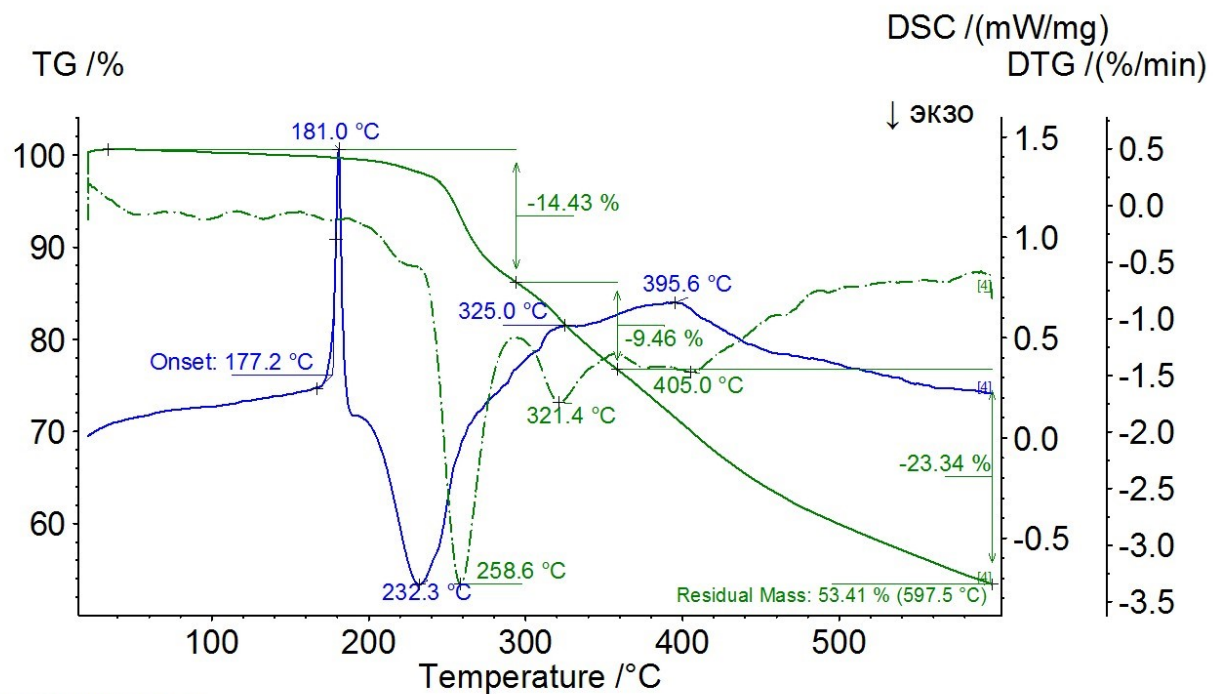


**Figure S10.** TGA/DSC traces for **1**.

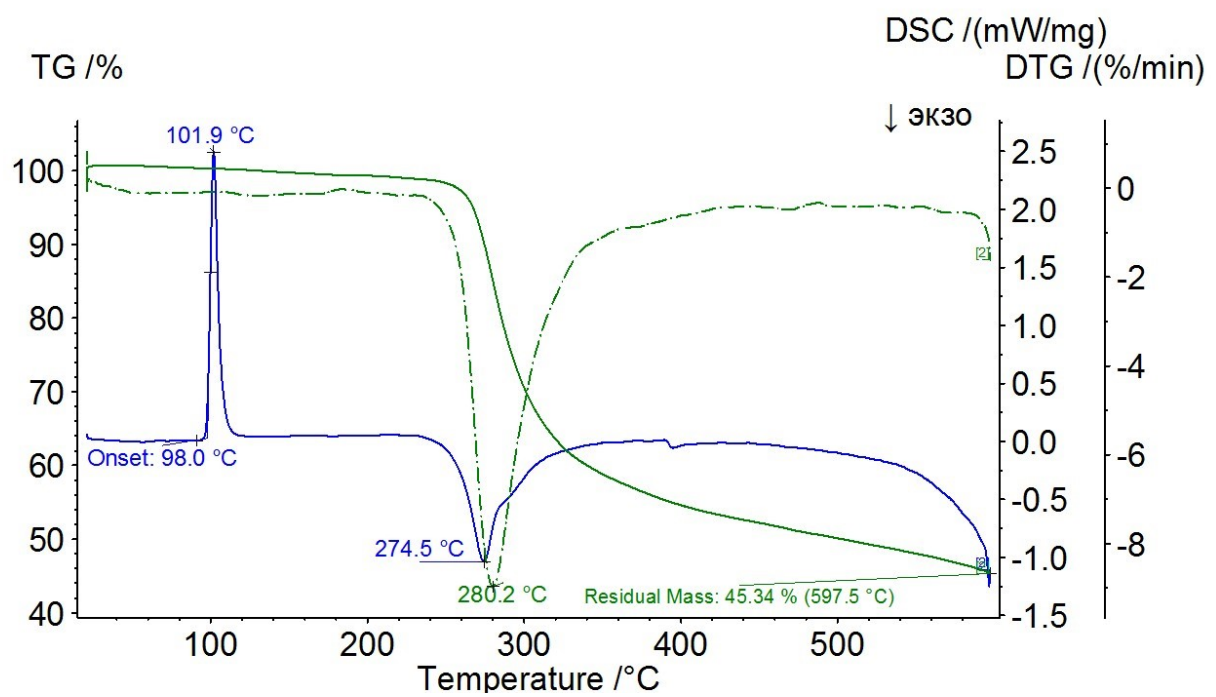


**Figure S11.** TGA/DSC traces for **2**.

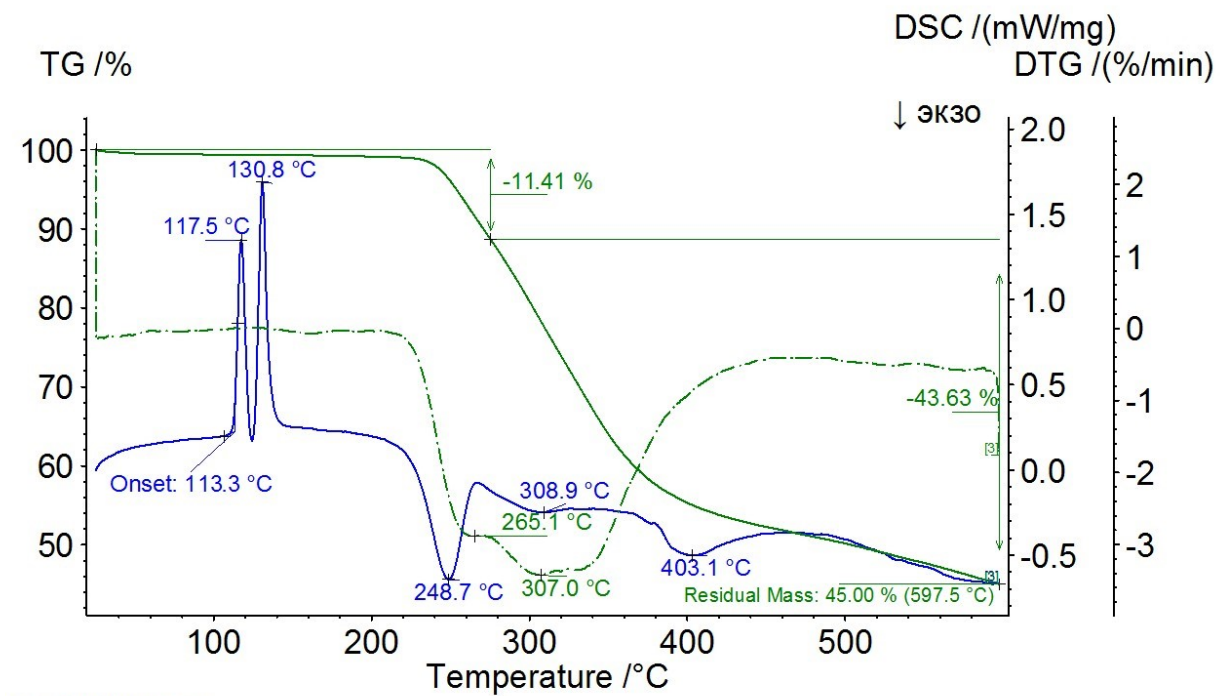


**Figure S12.** TGA/DSC traces for **3**.

#### 4. Synthesis of Fe(III) complexes

**1-Fe<sub>2</sub>** [C<sub>28</sub>H<sub>32</sub>Br<sub>2</sub>Cl<sub>2</sub>Fe<sub>2</sub>N<sub>2</sub>O<sub>8</sub>]: Compound **1** (25 mg, 0.044 mmol), FeCl<sub>3</sub>·6H<sub>2</sub>O (36.0 mg, 0.133 mmol) and triethylamine (24.7 µl, 0.178 mmol) were dissolved in CHCl<sub>3</sub>/MeOH mixture (v/v = 1/1, 10 ml). The obtained solution was stirred at room temperature for 1 hour then filtered off. The dark purple monocrystals, suitable for X-ray diffraction, were obtained upon slow vapor diffusion of isopropanol into the mother liquor at room temperature after 1 week. Total yield: 27 mg (72%, according to ligand **1**). MALDI-MS, m/z: 673.9 [M-4(OMe)-2Cl]<sup>+</sup> (m/z<sub>calc</sub> = 671.8); m/z: 615.9 [M-4(OMe)-Fe-2Cl]<sup>+</sup> (m/z<sub>calc</sub> = 615.9). IR (KBr, cm<sup>-1</sup>), v: 3423(m), 3055(w), 3007(w), 2926(s), 2855(m), 1745(m), 1618(s), 1585(m), 1544(m), 1461(s), 1440(m), 1395(m), 1346(m), 1333(s), 1300(m), 1249(s), 1210(m), 1120(w), 1099(w), 1036(m). 1003(m), 982(m), 943(w), 878(w), 864(w), 841(w), 810(w), 799(w), 790(w), 757(m), 738(w), 705(w), 692(w), 648(w), 580(w), 492(m), 466(m), 440(m), 440(m), 404(w). Elemental Analysis found: C, 38.68 %; H, 3.77 %; N, 3.32 %, calc. for [C<sub>28</sub>H<sub>32</sub>Br<sub>2</sub>Cl<sub>2</sub>Fe<sub>2</sub>N<sub>2</sub>O<sub>8</sub>]: C, 38.79 %; H, 3.72 %; N, 3.23 %.

**2<sub>2</sub>-Fe<sub>2</sub>** [C<sub>46</sub>H<sub>42</sub>Fe<sub>2</sub>N<sub>4</sub>O<sub>6</sub>]: In crystallization tube with diameter of 10 mm, a CHCl<sub>3</sub> solution (2 ml), containing dissolved compound **2** (25 mg, 0.073 mmol) and triethylamine (0.1 ml, 0.726 mmol), was layered by CHCl<sub>3</sub>/MeOH mixture (v/v = 1/1, 1 ml). Then, a MeOH solution (2 ml) of FeCl<sub>3</sub>·6H<sub>2</sub>O (39.2 mg, 0.145 mmol) was carefully added. The brownish red monocrystals, suitable for X-ray diffraction, were obtained upon slow diffusion after 1 week. Total yield: 24 mg (78%, according to ligand **2**). MALDI-MS, m/z: 796.2 [M-2(OMe)]<sup>+</sup> (m/z<sub>calc</sub> = 796.1); m/z: 398.1 [M-2(OMe)]<sup>2+</sup> (m/z<sub>calc</sub> = 398.1). IR (KBr, cm<sup>-1</sup>), v: 3443(m), 1616(m), 1542(m), 1496(w), 1470(m), 1447(m), 1399(m), 1319(m), 1198(m), 1149(m), 1127(m), 1065(w), 1037(m), 1015(w), 907(m), 855(w), 804(m), 768(m). Elemental Analysis found: C, 64.27 %; H, 5.02 %; N, 6.58 %, calc. for [C<sub>46</sub>H<sub>42</sub>Fe<sub>2</sub>N<sub>4</sub>O<sub>6</sub>]: C, 64.35 %; H, 4.93 %; N, 6.53 %.

**3<sub>2</sub>-Fe<sub>2</sub>** [C<sub>50</sub>H<sub>50</sub>Fe<sub>2</sub>N<sub>4</sub>O<sub>10</sub>] 2CHCl<sub>3</sub>: Compound **3** (25 mg, 0.062 mmol), FeCl<sub>3</sub>·6H<sub>2</sub>O (43 mg, 0.185 mmol) and triethylamine (34.4 µl, 0.247 mmol) were dissolved in CHCl<sub>3</sub>/MeOH mixture (v/v = 1/1, 10 ml). The obtained solution was stirred at room temperature for 1 hour then filtered off. The brownish red monocrystals, suitable for X-ray diffraction, were obtained upon slow evaporation of the mother liquor at room temperature under aerobic conditions after 2 weeks. Total yield: 23 mg (69%, according to ligand **3**). MALDI-MS, m/z: 916.2 [M-2(OMe)]<sup>+</sup> (m/z<sub>calc</sub> = 916.2), 393.2 [M-2(OMe)+Na]<sup>+</sup> (m/z<sub>calc</sub> = 393.2), 955.2 [M-2(OMe)+K]<sup>+</sup> (m/z<sub>calc</sub> = 955.1), 458.0 [M-2(OMe)]<sup>2+</sup> (m/z<sub>calc</sub> = 458.1), 481.0 [M-2(OMe)+Na]<sup>2+</sup> (m/z<sub>calc</sub> = 481.1), 497.0 [M-2(OMe)+K]<sup>2+</sup> (m/z<sub>calc</sub> = 497.0). IR (KBr, cm<sup>-1</sup>), v: 3442(m), 3055(m), 2925(m), 2820(m), 1616(s), 1544 (m), 1449(s), 1321(m), 1247(m), 1225(m), 1199(m), 1083(w), 1043(m), 862(m), 745(m), 667(m). Elemental Analysis found: C, 61.42 %; H, 5.12 %; N, 5.85 %, calc. for [C<sub>50</sub>H<sub>50</sub>Fe<sub>2</sub>N<sub>4</sub>O<sub>10</sub>] 2CHCl<sub>3</sub>: C, 51.30 %; H, 4.31 %; N, 4.60 %.

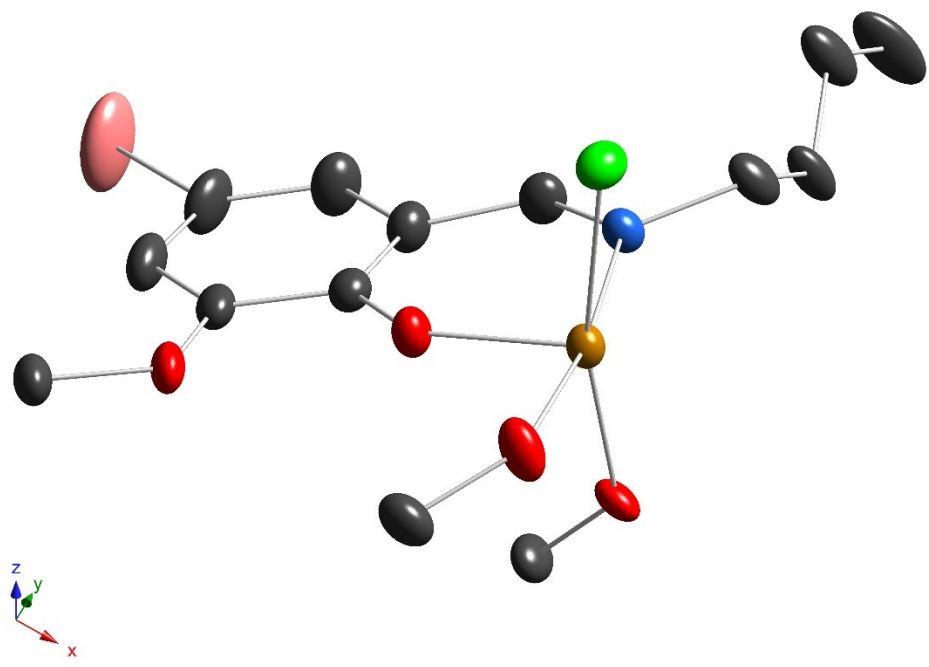
## 5. Single crystal X-ray diffraction analysis of Fe(III) complexes

X-ray diffraction study of the single crystals **1-Fe<sub>2</sub>**, **2<sub>2</sub>-Fe<sub>2</sub>** and **3<sub>2</sub>-Fe<sub>2</sub>** were collected on a Bruker D8 QUEST three-circle diffractometer (Bruker, Germany) with a PHOTON III area detector and an  $\text{I}\mu\text{S}$  DIAMOND microfocus X-ray tube (Incoatec, Germany) at a temperature of 150(2) K and 102(2) K for **1-Fe<sub>2</sub>**, **3<sub>2</sub>-Fe<sub>2</sub>** and **2<sub>2</sub>-Fe<sub>2</sub>**, respectively, the graphite monochromator,  $\lambda(\text{MoK}\alpha) = 0.71073 \text{ \AA}$ ,  $\omega/\phi$  scanning mode with a step of 0.5°. Data collection and indexing, determination, and refinement of unit cell parameters were carried out using the *APEX4* software package (v2021.10–0, Bruker AXS). Numerical absorption correction based on the crystal shape, additional spherical absorption correction, and systematic error correction were performed using the *SADABS*–2016/2 software.<sup>2</sup> Using *Olex2*,<sup>3</sup> structures were solved by direct methods using the *SHELXT*–2018/2 program<sup>4</sup> and refined by full-matrix least-squares on  $F^2$  using the *SHELXL*–2019/1 program.<sup>5</sup> Nonhydrogen atoms were refined anisotropically. The positions of hydrogen atoms of methyl groups were inserted using the rotation of the group with idealized bond angles. The remaining hydrogen atoms were refined using a riding model. Most calculations were performed using the *WinGX*–2021.3 software package.<sup>6</sup> The crystallographic data as well as the details of refinement procedure for **1-Fe<sub>2</sub>**, **2<sub>2</sub>-Fe<sub>2</sub>** and **3<sub>2</sub>-Fe<sub>2</sub>** are gathered in Table S1. The crystal of **1-Fe<sub>2</sub>** contains the voids of PLATON, filled by the highly disordered solvent molecules. A Solvent Mask, generated by the BYPASS module within *Olex2*,<sup>3</sup> was applied to calculate solvent accessible voids of 362 Å<sup>3</sup> with 113 electrons per unit cell, which is consistent with the presence of 11 H<sub>2</sub>O molecules. The crystallographic data are available for free of charge downloading from the Cambridge Crystallographic Data Centre via [www.ccdc.cam.ac.uk/datarequest/cif](http://www.ccdc.cam.ac.uk/datarequest/cif).

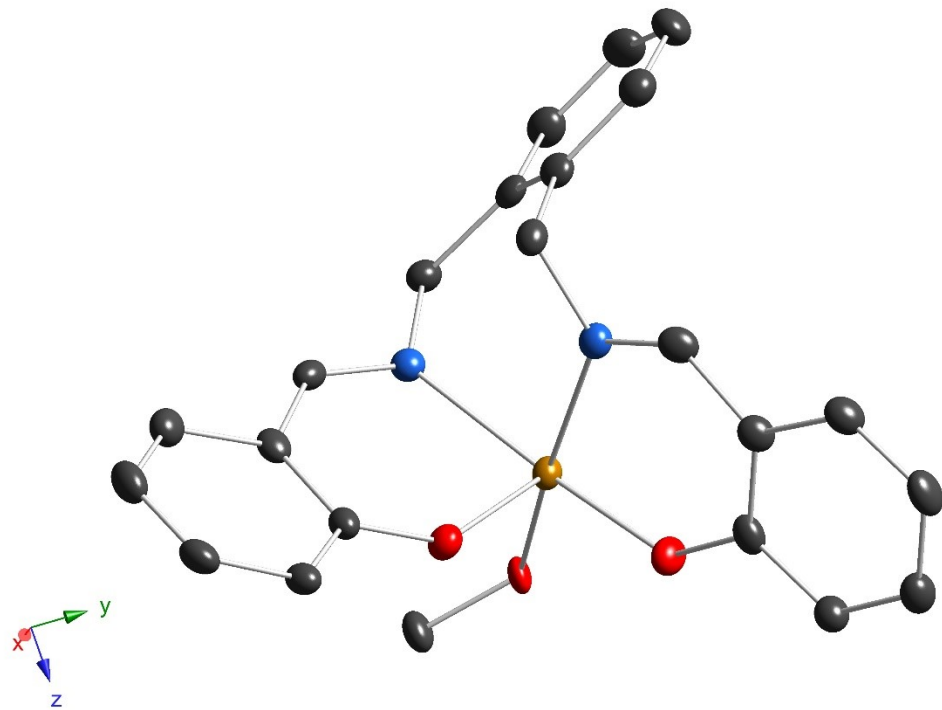
**Table 1.** Crystallographic data and X-ray structural experiment parameters for **1-Fe<sub>2</sub>**, **2<sub>2</sub>-Fe<sub>2</sub>** and **3<sub>2</sub>-Fe<sub>2</sub>**.

Compound	<b>1-Fe<sub>2</sub></b>	<b>2<sub>2</sub>-Fe<sub>2</sub></b>	<b>3<sub>2</sub>-Fe<sub>2</sub></b>
Empirical formula	C <sub>28</sub> H <sub>32</sub> Cl <sub>2</sub> Br <sub>2</sub> Fe <sub>2</sub> N <sub>2</sub> O <sub>8</sub> [+11H <sub>2</sub> O]	C <sub>46</sub> H <sub>42</sub> Fe <sub>2</sub> N <sub>4</sub> O <sub>6</sub>	C <sub>50</sub> H <sub>50</sub> Fe <sub>2</sub> N <sub>4</sub> O <sub>10</sub> , 2(CHCl <sub>3</sub> )
Formula weight	866.97	858.53	1217.37
Radiation, wavelength	MoK $\alpha$ , 0.71073 Å		
Temperature, K	150(2)	102(2)	150(2)
Crystal system	monoclinic		
Space group	P2/c (No. 13)	P2 <sub>1</sub> /c (No. 14)	P2 <sub>1</sub> /c (No. 14)
Unit cell dimensions: <i>a</i> , <i>b</i> , <i>c</i> , Å; $\beta$ , °	11.9195(13), 13.4258(14), 12.5162(13); 110.849(3)	11.0074(6), 15.0503(9), 11.4500(6); 96.275(2)	12.8712(7), 8.7624(5), 23.8209(13); 104.649(2)
Volume, Å <sup>3</sup>	1871.8(3)	1885.50(18)	2599.3(3)
Z and Z'	2 and 0.5		
Calculated density, g cm <sup>-3</sup>	1.538	1.512	1.555
Absorption coefficient, mm <sup>-1</sup>	3.096	0.828	0.930
<i>F</i> (000)	868	892	1252
Crystal size, mm <sup>3</sup>	0.408 × 0.076 × 0.064	0.119 × 0.08 × 0.078	0.437 × 0.087 × 0.041
$\theta$ range for data collection, °	2.309 to 25.998	2.243 to 26.000	1.767 to 26.999
Index ranges	-14 ≤ <i>h</i> ≤ 14, -16 ≤ <i>k</i> ≤ 16, -15 ≤ <i>l</i> ≤ 15	-13 ≤ <i>h</i> ≤ 13, -18 ≤ <i>k</i> ≤ 18, -14 ≤ <i>l</i> ≤ 14	-16 ≤ <i>h</i> ≤ 16, -11 ≤ <i>k</i> ≤ 11, -30 ≤ <i>l</i> ≤ 30
Reflections collected	35651	32043	113171
Independent reflections	3681	3713	5668
<i>R</i> <sub>int</sub>	0.0615	0.0909	0.0436
<i>R</i> <sub>σ</sub>	0.0299	0.0514	0.0144
Observed Data [ <i>I</i> > 2 $\sigma$ ( <i>I</i> )]	3058	3003	5496

Completeness to $\theta = 25.242^\circ$ , %	99.9	99.9	99.9
Max. and min. transmission	0.9281 and 0.7519	0.7460 and 0.6683	0.7460 and 0.6919
Data / restraints / parameters	3681 / 33 / 202	3713 / 0 / 263	5668 / 0 / 337
Goodness-of-fit on $F^2$	1.067	1.100	1.146
Final $R$ indices [ $I > 2\sigma(I)$ ]	$R1 = 0.0506$ , $wR2 = 0.1239$	$R1 = 0.0586$ , $wR2 = 0.1245$	$R1 = 0.0423$ , $wR2 = 0.0976$
$R$ indices (all data)	$R1 = 0.0609$ , $wR2 = 0.1298$	$R1 = 0.0779$ , $wR2 = 0.1324$	$R1 = 0.0436$ , $wR2 = 0.0983$
Largest diff. peak and hole, $e \text{ \AA}^{-3}$	1.449 and -1.014	0.623 and -0.479	1.184 and -0.900
CCDC number	2428629	2428627	2428628



a



b

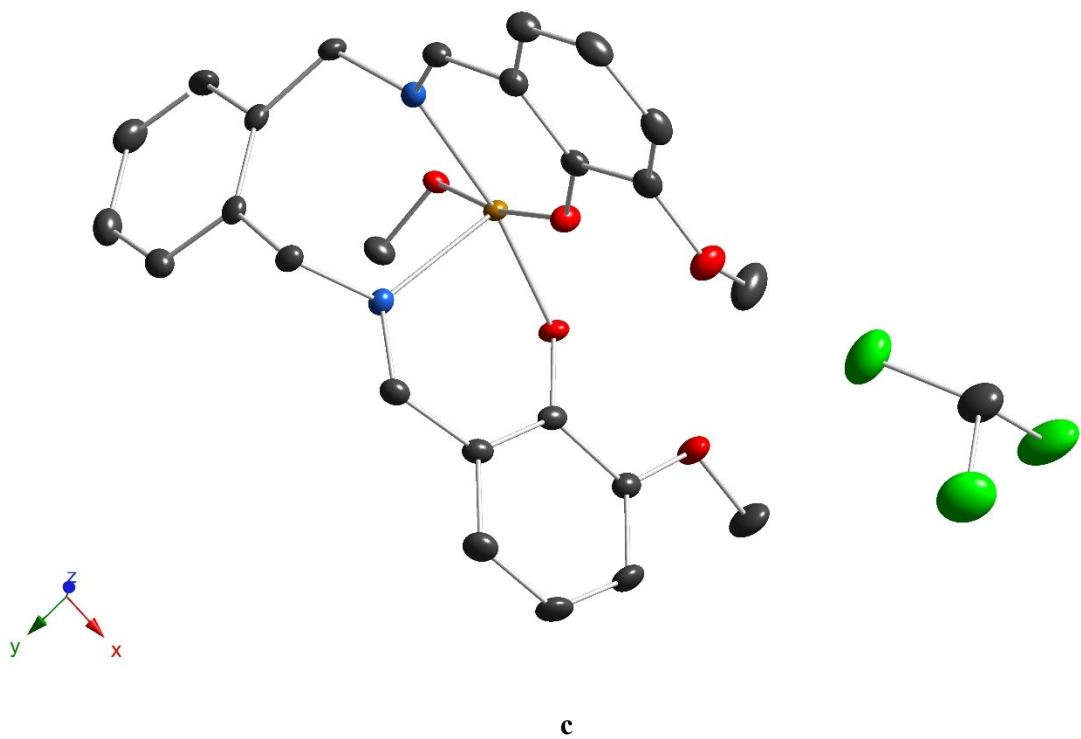
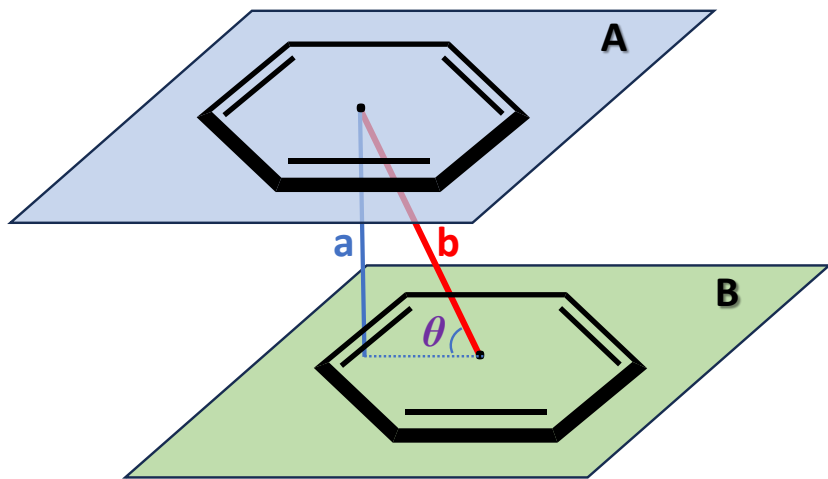


**Figure S13.** ORTEP view of asymmetric unit for molecular structure of **1-Fe<sub>2</sub>** (a), **2<sub>2</sub>-Fe<sub>2</sub>** (b) and **3<sub>2</sub>-Fe<sub>2</sub>** (c) with 50% probability. The C-, O-, N-, Cl-, Fe-, and Br-atoms are represented by dark grey, red, blue, green, goldish and rose spheres. The H-atoms are omitted for clarity.



$$\begin{aligned} \mathbf{a} &= 3.57(1) \text{ \AA} \\ \mathbf{b} &= 3.56(1) \text{ \AA} \\ \theta &= 84.5(1)^\circ \\ \angle A-B &= 10.9(2)^\circ \end{aligned}$$

**Figure S14.** For 1-Fe<sub>2</sub>, the schematic representation of the characteristic parameters of face-to-face π-bonding, observed between the salicylideneamine moieties.

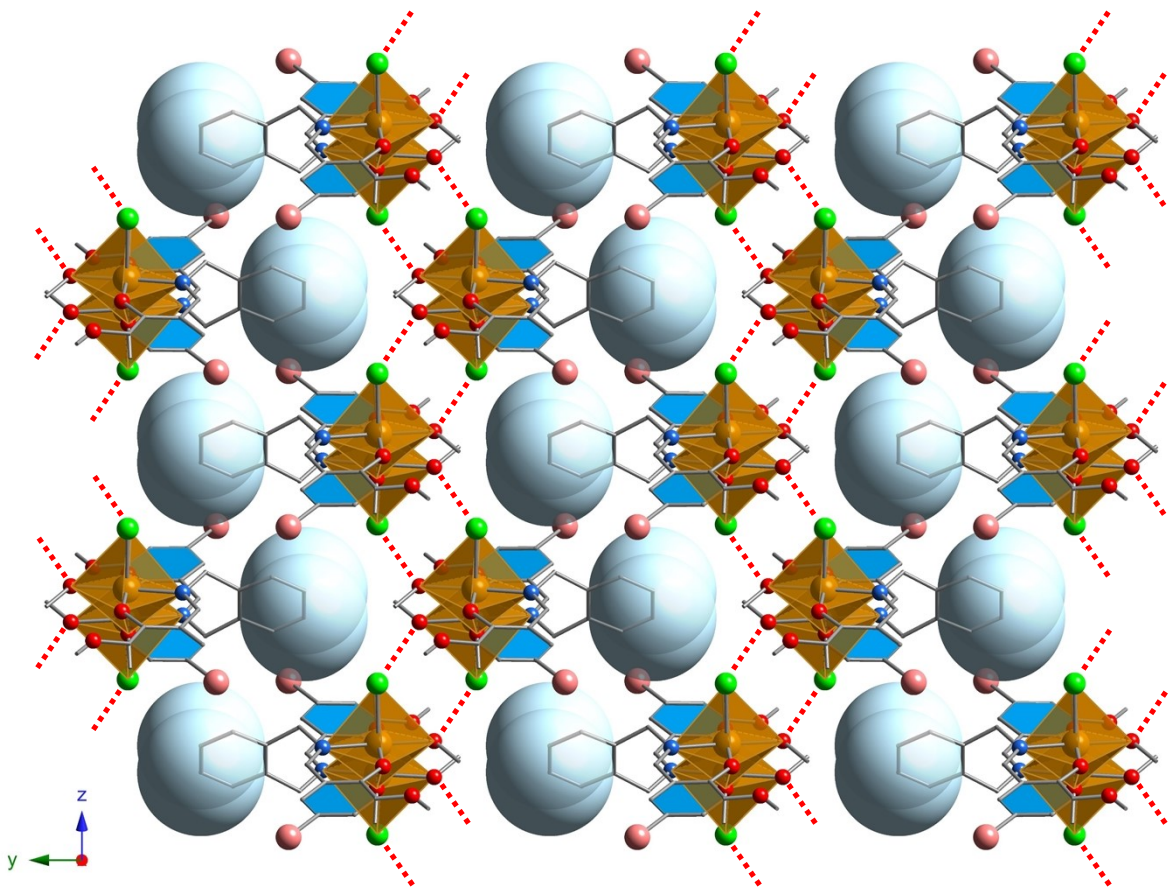


**Figure S15.** For **1-Fe<sub>2</sub>**, a fragment of crystal packing, showing the formation of the pores (translucent light blue spheres) upon the staking of the 2D molecular networks, resulting from the intermolecular  $\pi$ -bonding (the aryl units colored in blue) as well as nonclassical O/Cl H-bonding between the complex species. The C-, O-, N-, Cl-, Fe-, and Br-atoms are represented by dark grey, red, blue, green, goldish and rose spheres. The H-atoms are omitted for clarity.

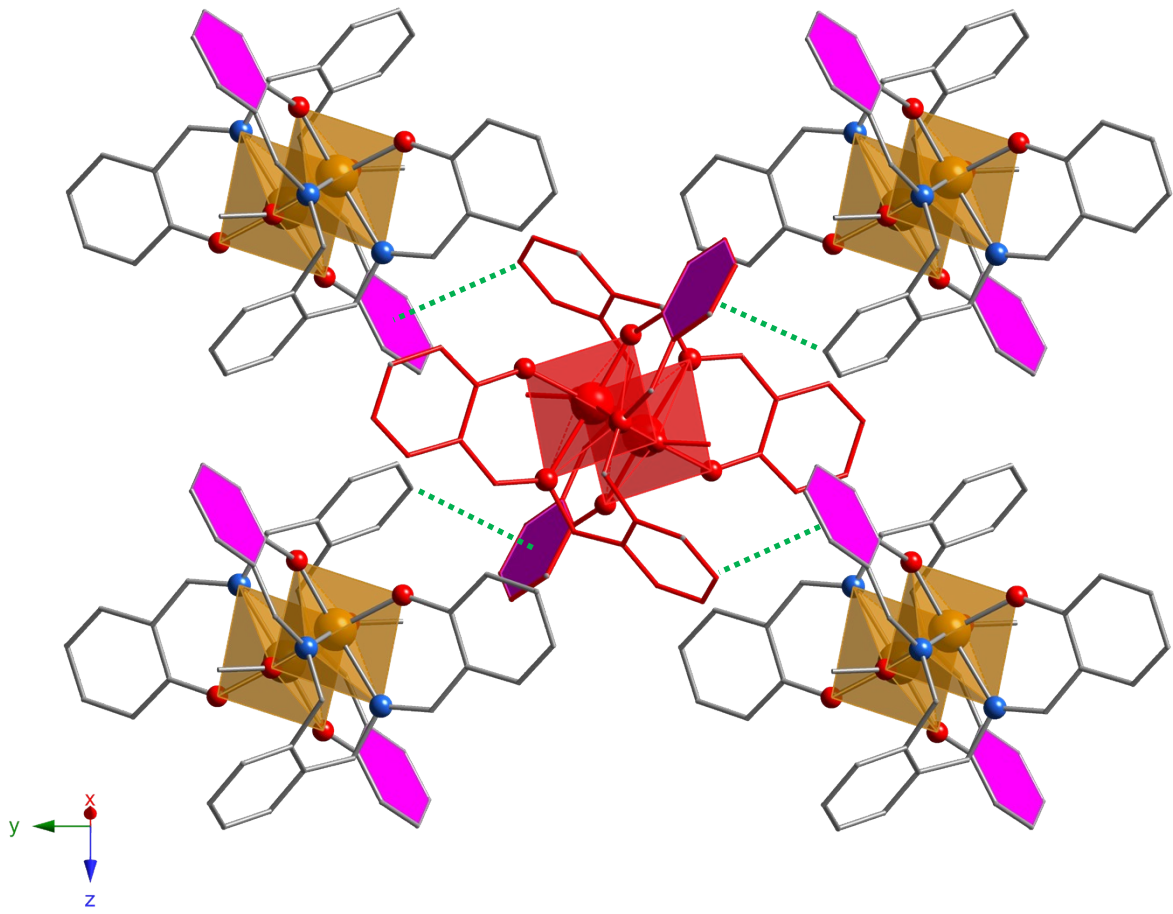


**Figure S16.** For  $\mathbf{2}_2\text{-Fe}_2$ , a fragment of the crystal packing, showing the intermolecular  $\text{CH}-\pi$  interaction (green dotted line), involving  $\text{C}(11)$ -atom of xylylene unit and aromatic salicylidene moiety, belonging to adjacent complex species ( $d_{\text{C}(11)\dots\text{C}6\text{centr}}=3.545(2) - 3.638(2)$  Å). The C-, O-, N-, and Fe-atoms are represented by dark grey, red, blue, and goldish spheres. The H-atoms are omitted for clarity.

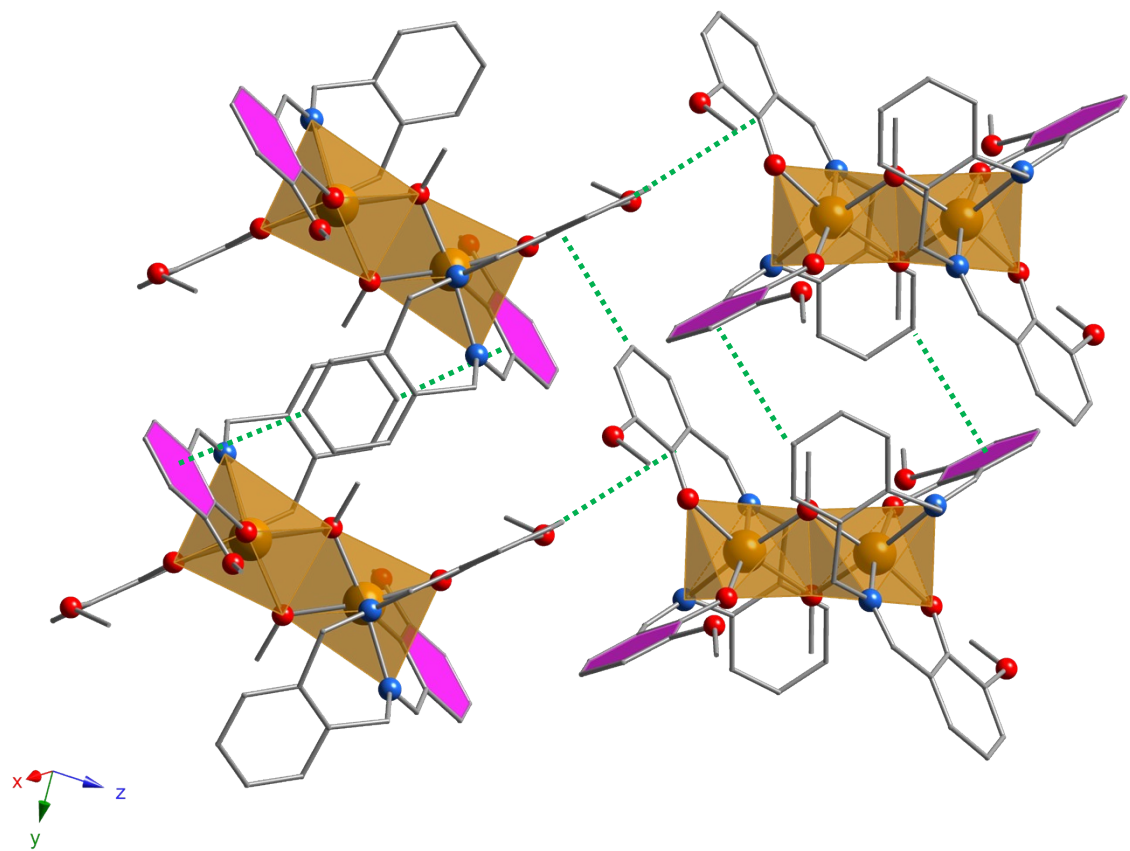


**Figure S17.** For  $3_2\text{-Fe}_2$ , a fraction of the crystal packing, showing the intermolecular  $\text{CH}/\pi$  interactions, involving complex species.

## 6. Characterization of Fe(III) complexes

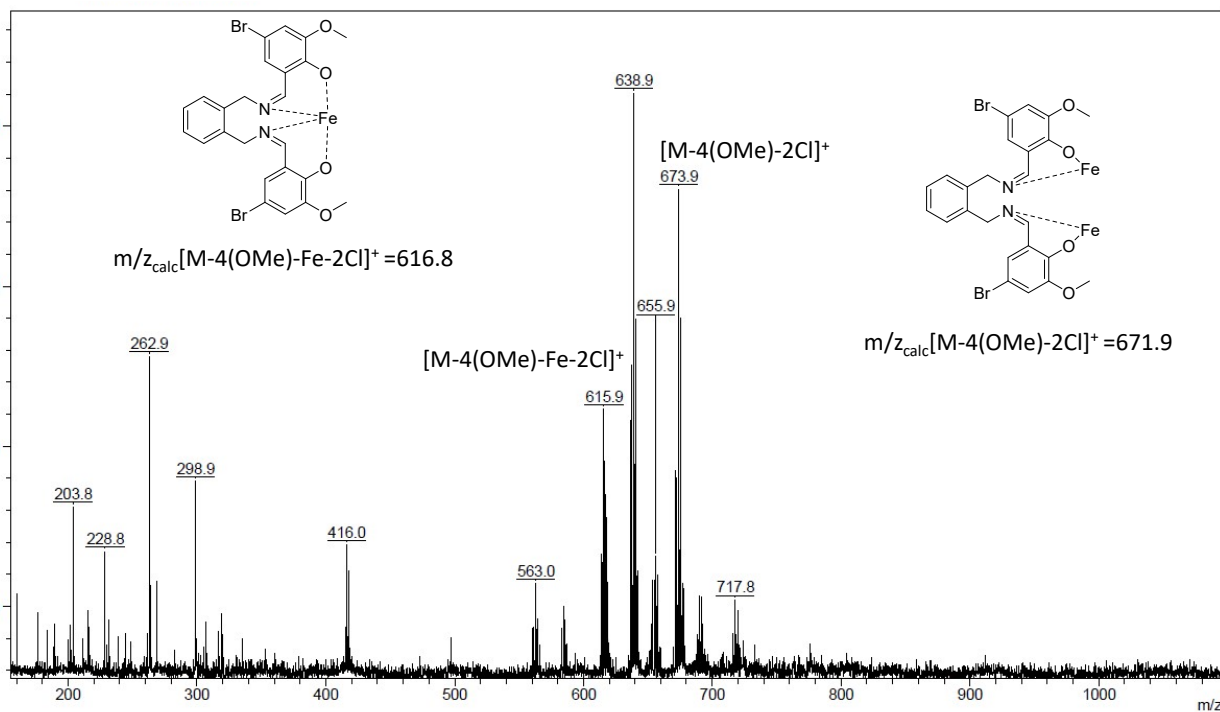


Figure S18. The MALDI-MS spectrum for **1-Fe<sub>2</sub>**.

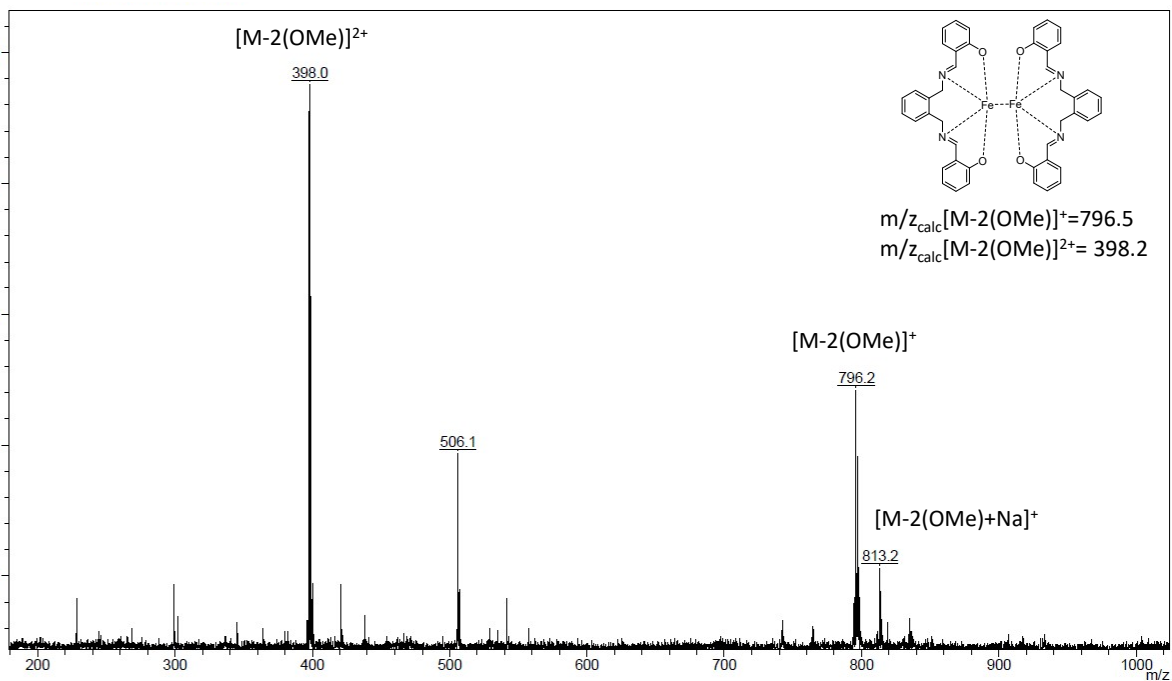
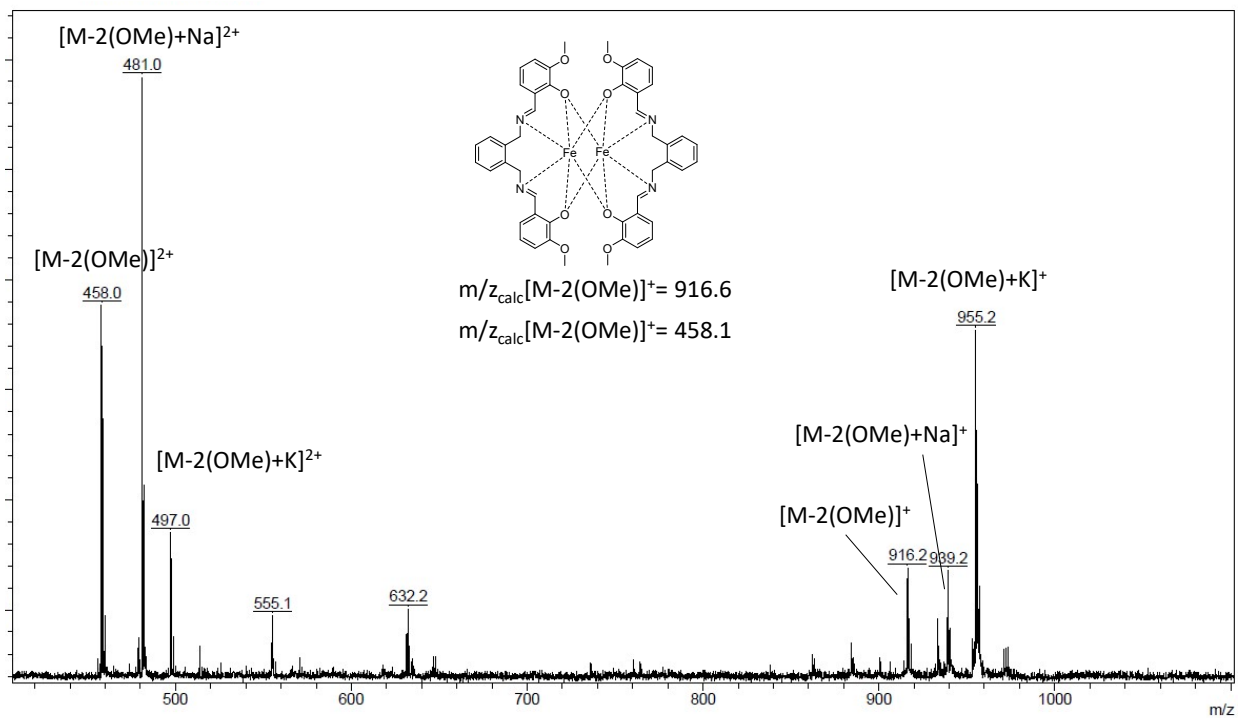
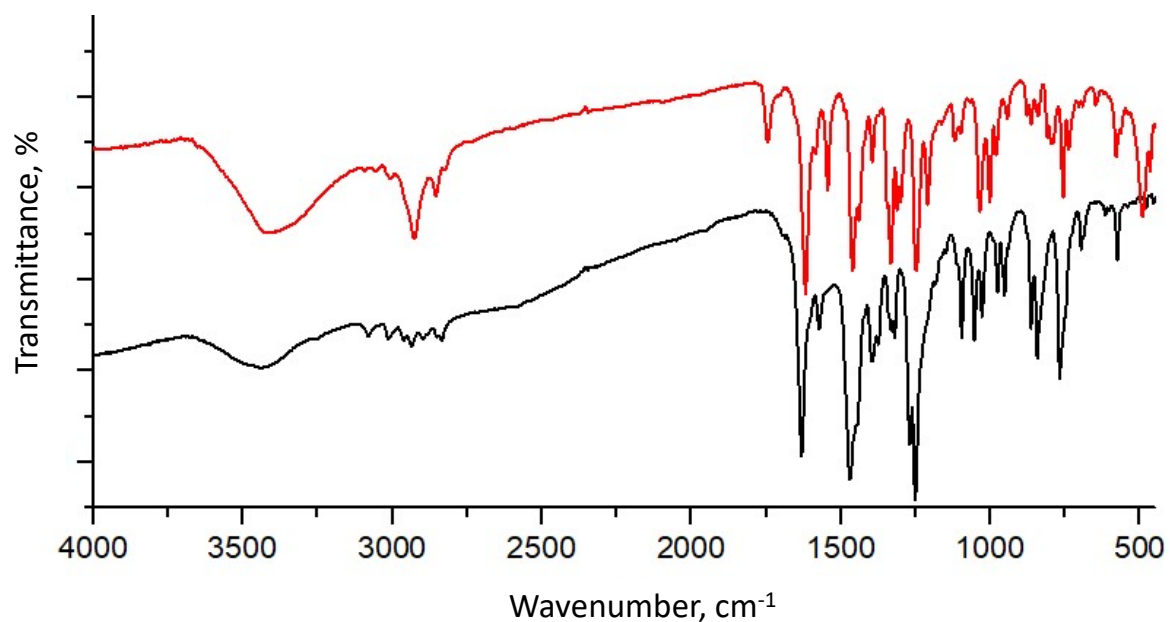


Figure S19. The MALDI-MS spectrum for **2<sub>2</sub>-Fe<sub>2</sub>**.



**Figure S20.** The MALDI-MS spectrum for **3<sub>2</sub>-Fe<sub>2</sub>**.



**Figure S21.** A comparison of IR spectra for free Schiff base ligand **1** (black line) with this one obtained for **1-Fe<sub>2</sub>** (red line).

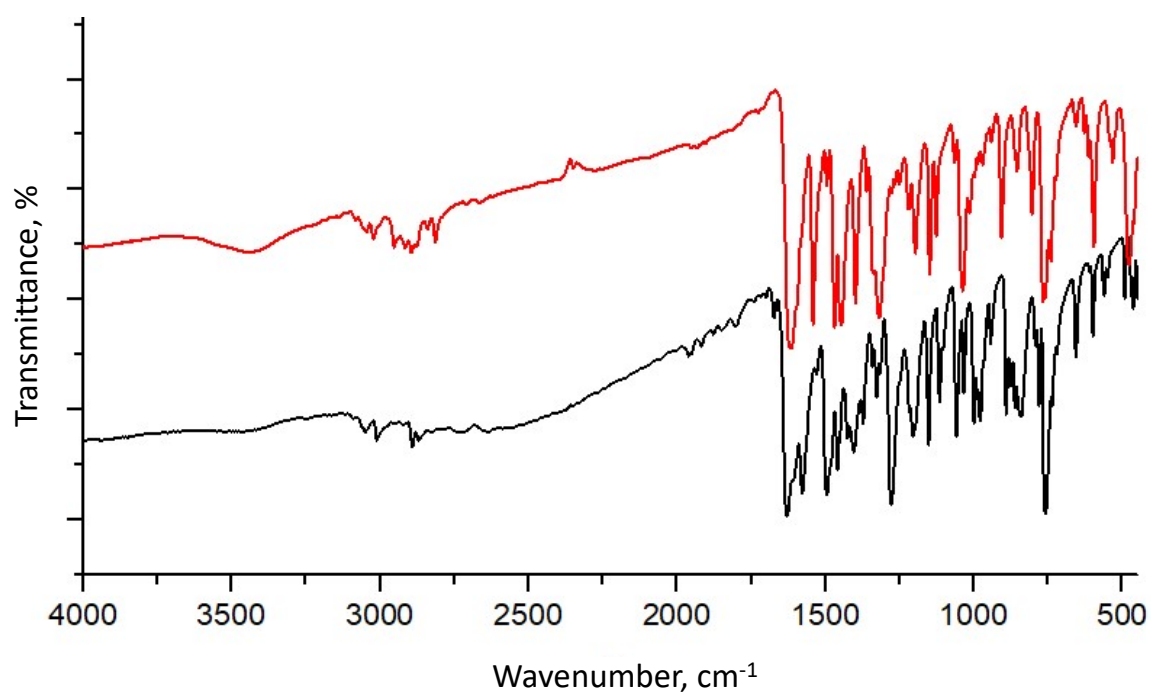


**Figure S22.** A comparison of IR spectra for free Schiff base ligand **2** (black line) with this one obtained for **2-Fe<sub>2</sub>** (red line).

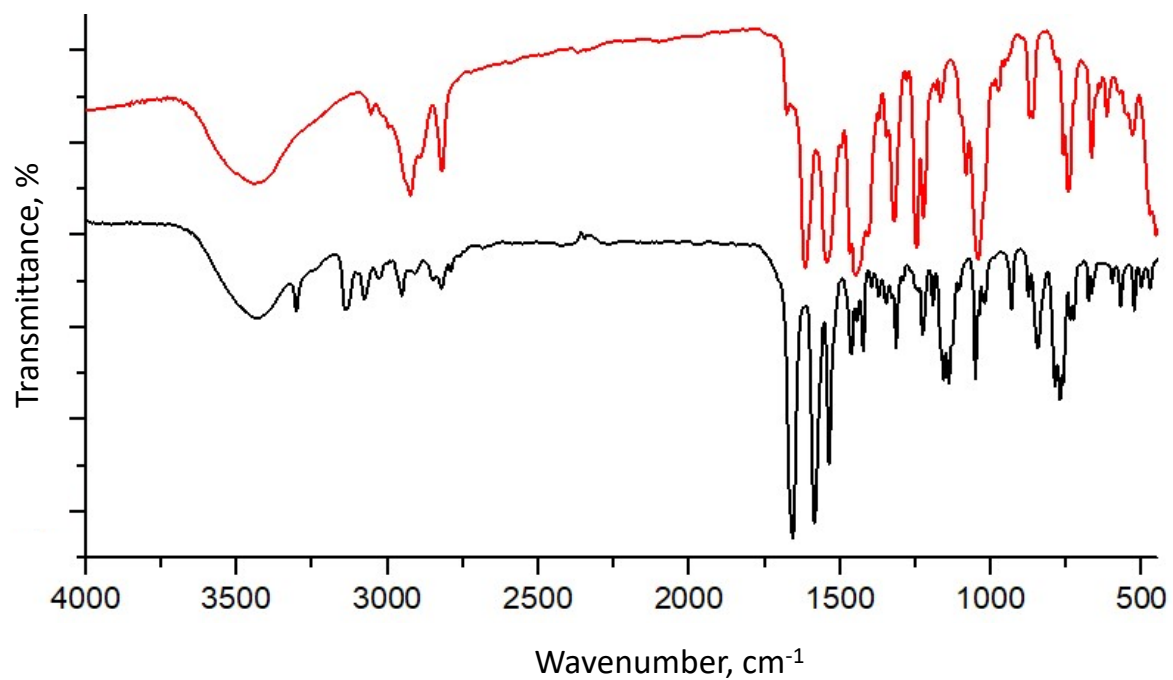


**Figure S23.** A comparison of IR spectra for free Schiff base ligand **3** (black line) with this one obtained for **3<sub>2</sub>-Fe<sub>2</sub>** (red line).

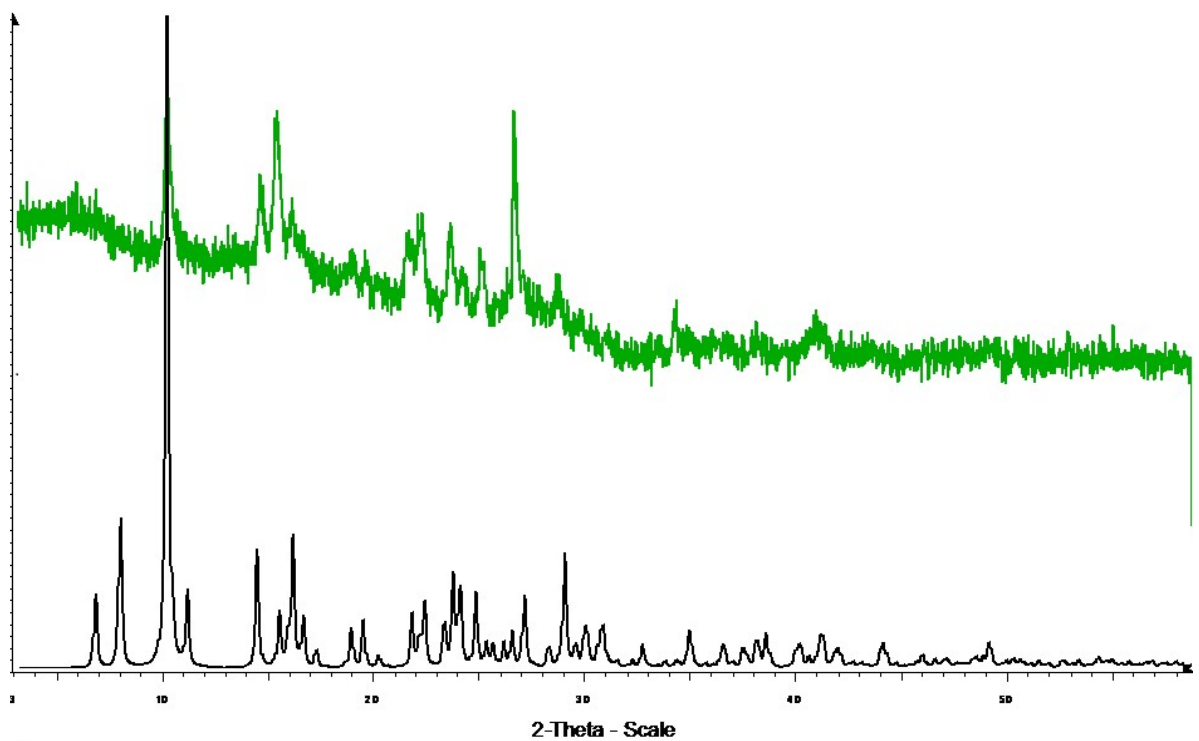


**Figure S24.** For  $1\text{-Fe}_2$ , a comparison of simulated PXRD pattern (black line) with the experimental one (green line). The experimental and simulated patterns demonstrate rather good matching. The broadening of the peaks evidences a partial loose of crystallinity (amorphization) of the sample after separation from the mother liquor.

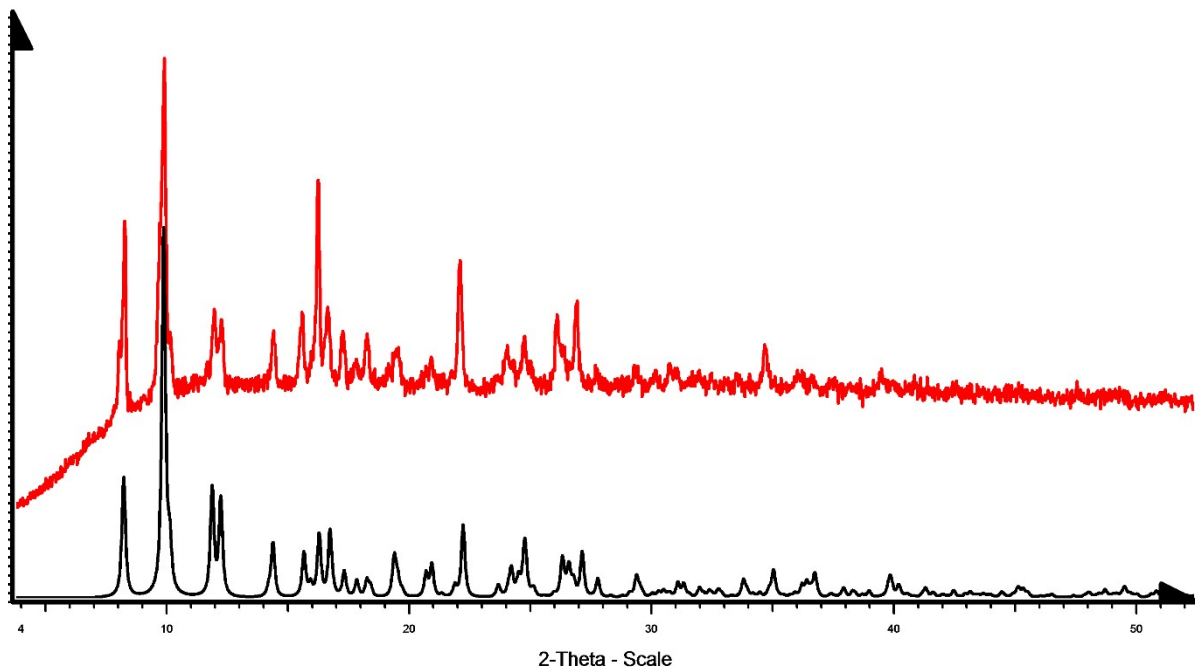


**Figure S25.** For  $2_2\text{-Fe}_2$ , a comparison of simulated PXRD pattern (black line) with the experimental one (red line).

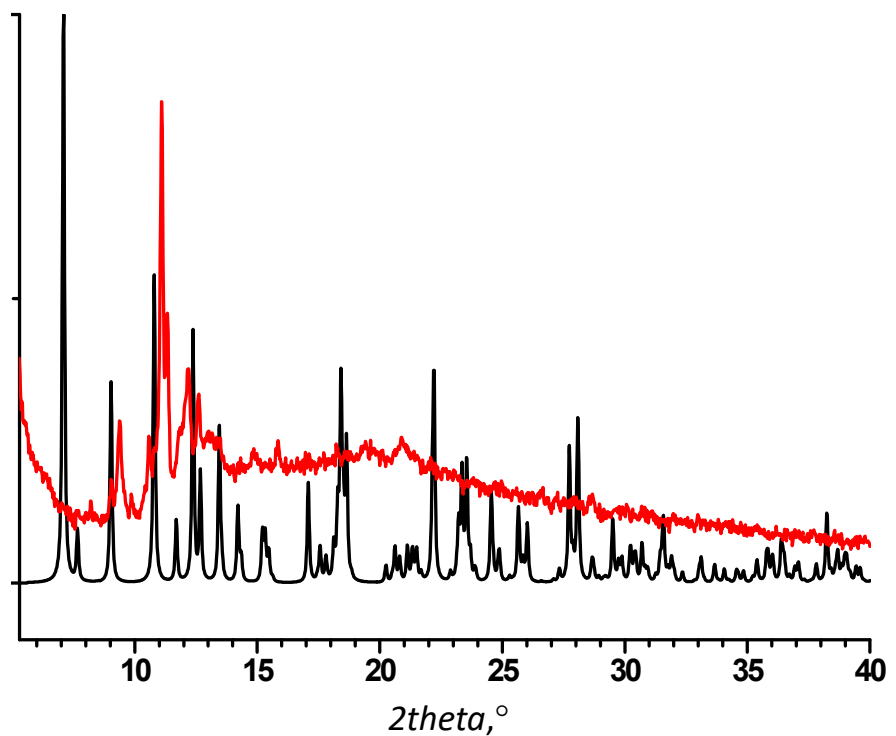


**Figure S26.** For  $\text{3}_2\text{-Fe}_2$ , a comparison of simulated PXRD pattern (black line) with the experimental one (redline). The mismatching between the experimental and simulated patterns is assumedly caused by fast release of the  $\text{CHCl}_3$  solvate molecules followed by solid – state transition.

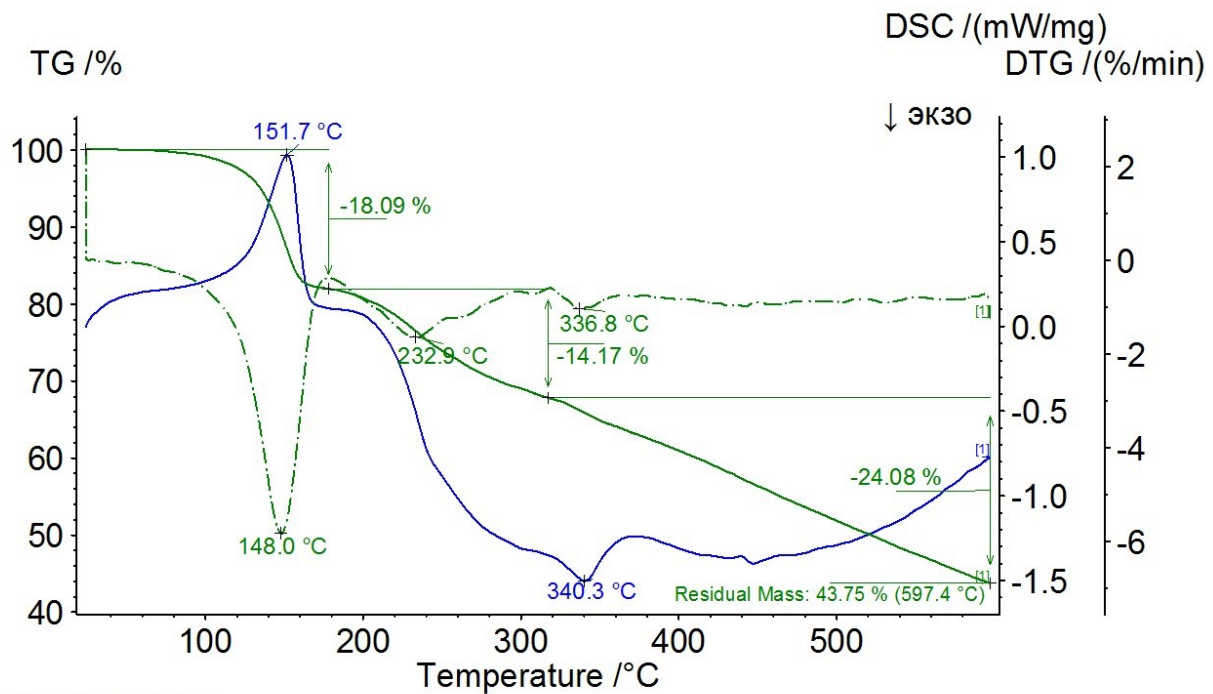


**Figure S27.** The TGA/DSC traces for **1-Fe<sub>2</sub>**. The mass loss of 18.09% in the temperature range from 25 to 180 °C corresponds to release of the 11 H<sub>2</sub>O solvent molecules, giving rise to formula [C<sub>28</sub>H<sub>32</sub>Br<sub>2</sub>Cl<sub>2</sub>Fe<sub>2</sub>N<sub>2</sub>O<sub>8</sub>]·11H<sub>2</sub>O, which is in accordance with the SCXRD data.

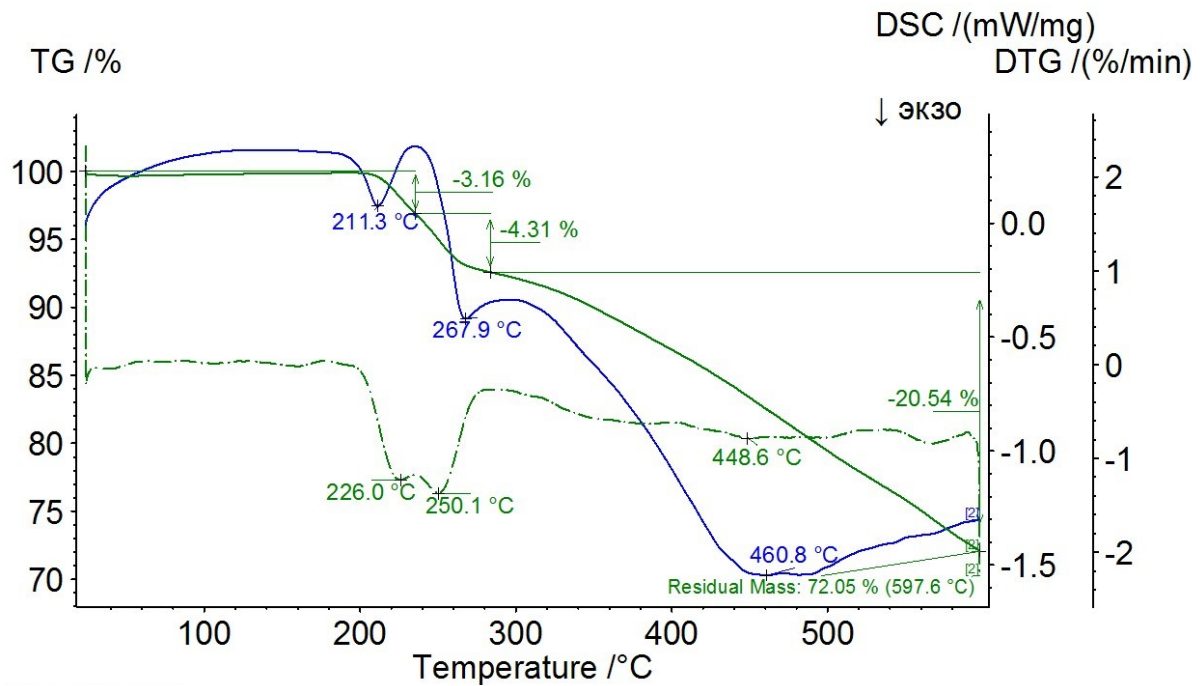


**Figure S28.** The TGA/DSC traces for **2<sub>2</sub>-Fe<sub>2</sub>**.

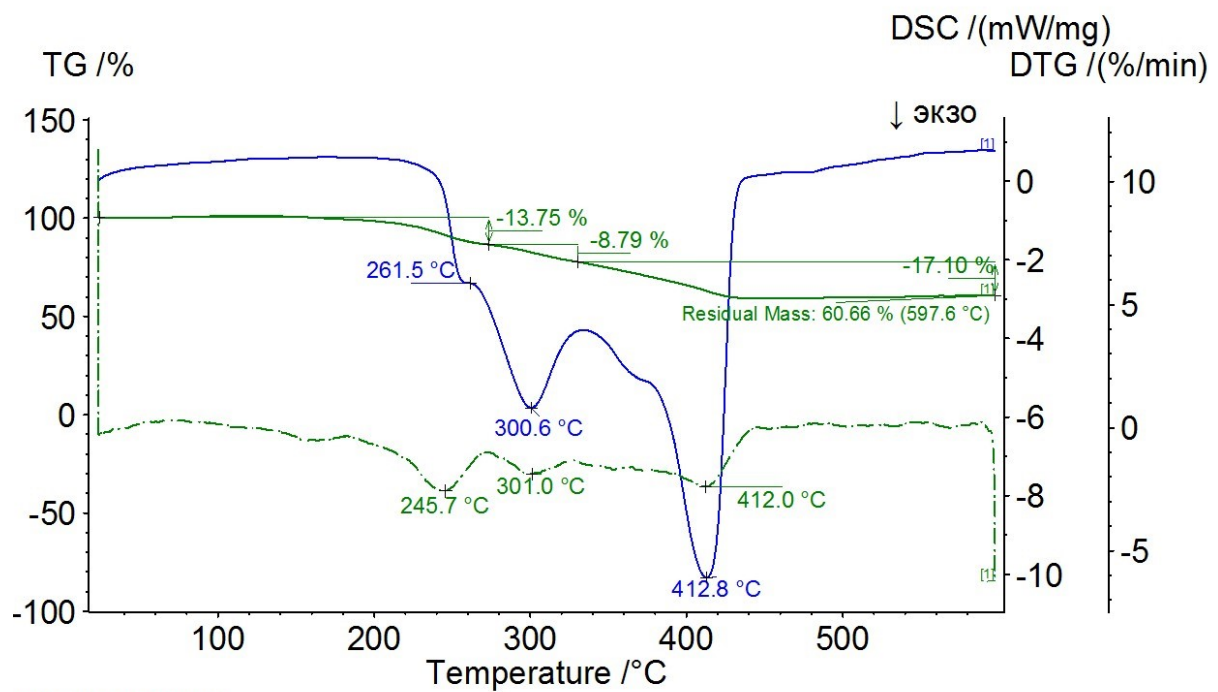


**Figure S29.** The TGA/DSC traces for  $\mathbf{3}_2\text{-Fe}_2$ .

## 7. Structural parameters for Fe(III) complexes

**Table S2.** The coordination bond lengths and angles for **1-Fe<sub>2</sub>**, **2<sub>2</sub>-Fe<sub>2</sub>** and **3<sub>2</sub>-Fe<sub>2</sub>**, according to SCXRD.

	<b>1-Fe<sub>2</sub></b>	<b>2<sub>2</sub>-Fe<sub>2</sub></b>	<b>3<sub>2</sub>-Fe<sub>2</sub></b>
d (Fe...N), Å	2.129(3)	2.170(3) 2.191(3)	2.171(2) 2.177(2)
d (Fe...O <sub>x</sub> ), Å	1.904(2) 2.017(2) 2.112(3) 1.994(3)	1.940(3) 2.033(2) 1.998(2) 1.947(3)	1.940(1) 2.002(2) 2.003(2) 1.943(2)
d (Fe...Cl), Å	2.379(1)	-	-
∠ N <sub>x</sub> –Fe–N <sub>y</sub> , °	-	84.6(1)	83.19(7)
∠ N <sub>x</sub> –Fe–Cl, °	90.2(1)	-	-
∠ N <sub>x</sub> –Fe–O <sub>x</sub> , °	97.9(1) 171.8(1) 86.2(1) 89.5(1)	93.4(1) 167.6(1) 95.1(1) 92.3(1) 94.0(1) 84.9(1)	85.66(7) 168.9(1) 98.42(7) 171.93(7) 90.18(7) 92.16(7) 92.54(7) 85.18(7)
∠ O <sub>x</sub> –Fe–O <sub>y</sub> , °	90.1(1) 167.9(1) 73.9(1) 86.3(1) 94.3(1) 94.9(1)	94.0(1) 96.4(1) 90.2(1) 74.31(9) 170.7(1) 97.1(1)	93.04(7) 98.96(7) 91.26(7) 74.82(6) 170.64(7) 96.30(7)
∠ O <sub>x</sub> –Fe–Cl, °	92.39(8) 87.9(1) 98.96(8) 166.13(8)		
d (Fe...Fe), Å	3.203(1)	3.2131(8)	3.1811(7)

**Table S3.** The coordination octahedrons distortions of Fe(III) atoms for **1-Fe<sub>2</sub>**, **2<sub>2</sub>-Fe<sub>2</sub>** and **3<sub>2</sub>-Fe<sub>2</sub>**, calculated by *OctaDist* program.<sup>7</sup>

Complex	<i>d<sub>mean</sub></i> , Å	$\zeta$ , Å	$\Delta$	$\Sigma$ , °	$\Theta$ , °
<b>1-Fe<sub>2</sub></b>	2.0871	0.713830	0.005238	54.4879	197.1960
<b>2<sub>2</sub>-Fe<sub>2</sub></b>	2.0465	0.535703	0.002383	62.7901	193.9150
<b>3<sub>2</sub>-Fe<sub>2</sub></b>	2.0395	0.538836	0.002329	64.0091	196.2033

*d<sub>mean</sub>*- average metal-ligand distances, Å;

$\zeta$ - stretching distortion, Å;

$\Delta$  - tilting distortion, Å;

$\Sigma$  - angular distortion, °;

$\Theta$ - torsional distortion, °

## 8. DFT study of complexes

The calculations of geometry models and frontier orbital energy for **1-Fe<sub>2</sub>**, **2<sub>2</sub>-Fe<sub>2</sub>** and **3<sub>2</sub>-Fe<sub>2</sub>** were performed using GAUSSIAN 09 program package.<sup>8</sup> The molecular geometry optimizations were carried out at the density functional theory (DFT) with the Lee Yang Parr functional correlation (B3LYP).<sup>9,10</sup> For the ligand atoms (H, C, O, N, Cl, and Br), the 6-31+G\* basis set was employed, while the metal (Fe) atom was treated with the Hay and Wadt (LanL2DZ) double-zeta effective core potential (ECP) basis set. The obtained Fe(III)-complexes were calculated as neutral molecules with a multiplicity of 11.

**Table S4.** Optimized geometries in Cartesian coordinates for **1-Fe<sub>2</sub>**, obtained by DFT-B3LYP calculations.

Center Number	Atomic Number	Coordinates (Angstroms)		
		X	Y	Z
1	35	8,00206	2,30864	-0,10795
2	26	1,36522	-1,17904	-0,653
3	17	2,0283	-1,65221	-2,92299
4	8	0,5549	-1,33229	1,16476
5	8	3,17227	-1,30073	0,0243
6	8	1,2741	-3,59841	-0,74713
7	8	5,53545	-2,32227	0,59252
8	7	1,6513	0,9292	-0,79715
9	6	0,50609	1,77693	-1,23265
10	1	0,68581	2,07731	-2,27179
11	6	1,19481	-1,67034	2,38798
12	1	0,8658	-2,66115	2,72336
13	1	0,92021	-0,94748	3,16573
14	1	2,28044	-1,66733	2,24683
15	6	0,24205	3,00755	-0,38356
16	6	6,79415	-2,90148	0,91486
17	1	7,23712	-2,4244	1,79894
18	1	7,49171	-2,83279	0,06995
19	1	6,58948	-3,95092	1,13282
20	6	5,49691	-0,99887	0,27818
21	6	4,18983	-0,49465	-0,03542
22	6	2,81174	1,49745	-0,70383
23	1	2,86997	2,57432	-0,89836
24	6	6,60512	-0,1652	0,24596
25	1	7,59315	-0,54383	0,47612
26	6	4,07482	0,88403	-0,37333
27	6	6,45295	1,19437	-0,08791
28	6	2,26424	-4,37717	-0,03941
29	1	1,92942	-4,43293	0,99752
30	1	3,23748	-3,88193	-0,0842
31	1	2,31733	-5,38639	-0,46243
32	6	5,21957	1,72186	-0,39003
33	1	5,11292	2,77176	-0,64379
34	6	0,49917	4,27726	-0,91548
35	6	0,25259	5,44146	-0,18031
36	1	0,46206	6,41428	-0,61718
37	35	-7,88423	2,38946	-0,38159
38	8	-3,21984	-1,41335	0,04113
39	8	-5,54443	-2,34295	-0,77018
40	7	-1,70158	0,78305	0,97725
41	6	-0,57726	1,56036	1,56325

42	1	0,30058	0,91775	1,49684
43	1	-0,79103	1,69352	2,63041
44	6	-0,29229	2,90648	0,92304
45	6	-6,78699	-2,88196	-1,20243
46	1	-7,12461	-2,40899	-2,13422
47	1	-7,56011	-2,76915	-0,43107
48	1	-6,60278	-3,94285	-1,3796
49	6	-5,48567	-1,01822	-0,46919
50	6	-4,19959	-0,56027	-0,0246
51	6	-2,8229	1,39216	0,77307
52	1	-2,87072	2,46832	0,97477
53	6	-6,55813	-0,14208	-0,56461
54	1	-7,53054	-0,48692	-0,89331
55	6	-4,06515	0,81838	0,30461
56	6	-6,38726	1,21421	-0,23176
57	6	-5,17098	1,69828	0,19173
58	1	-5,05031	2,74672	0,44543
59	6	-0,53067	4,07921	1,65005
60	6	-0,26072	5,34154	1,11122
61	1	-0,45571	6,23537	1,69787
62	26	-1,4653	-1,35805	0,82308
63	17	-2,08034	-1,66536	3,0483
64	8	-0,56329	-1,18506	-1,06285
65	8	-1,21099	-3,49887	0,53758
66	6	-1,29578	-1,20668	-2,27793
67	1	-0,60745	-1,20235	-3,1284
68	1	-1,95722	-0,33118	-2,3383
69	1	-1,92519	-2,104	-2,32393
70	6	-2,28195	-4,44559	0,41871
71	1	-2,95518	-4,25754	1,25561
72	1	-1,88332	-5,46416	0,48713
73	1	-2,82609	-4,30779	-0,52129
74	1	-0,93155	4,00251	2,65873
75	1	0,89331	4,35727	-1,92668
76	1	-0,36656	1,12622	-1,23343
77	1	-0,48361	-3,66618	-0,10072
78	1	1,53216	-3,51389	-1,69087

**Table S5.** Optimized geometries in Cartesian coordinates for  $\text{2}_2\text{-Fe}_2$ , obtained by DFT-B3LYP calculations.

Center Number	Atomic Number	Coordinates (Angstroms)		
		X	Y	Z
1	26	1,59689	0,02747	-0,03201
2	8	1,8984	0,209	1,893
3	8	-0,02223	1,23965	-0,22882
4	8	2,90255	1,42569	-0,45801
5	7	3,23536	-1,51954	0,07698
6	7	1,69747	-0,45219	-2,20034
7	6	1,29721	-2,96971	-2,15555
8	6	3,08751	1,47024	-2,85271
9	6	2,48144	-3,31791	-1,47731
10	6	2,90684	-0,02439	2,68941
11	6	3,38332	1,96695	-1,54202
12	6	2,26645	0,30624	-3,08112
13	1	2,14811	0,03636	-4,13994

14	6	3,98278	-0,89983	2,33894
15	6	0,93288	-1,59388	-2,70291
16	1	1,01369	-1,62884	-3,80239
17	1	-0,11804	-1,40294	-2,4638
18	6	4,23729	3,0979	-1,43945
19	1	4,46071	3,46595	-0,4422
20	6	4,0535	-1,59407	1,07502
21	1	4,92455	-2,25712	0,9771
22	6	3,57305	-2,32621	-1,10935
23	1	4,50063	-2,8846	-0,921
24	1	3,77514	-1,63904	-1,93301
25	6	-0,05535	2,373	-1,07834
26	1	0,81111	3,01328	-0,87997
27	1	-0,96706	2,95222	-0,89726
28	1	-0,04248	2,06803	-2,13384
29	6	2,67245	-4,65487	-1,08645
30	1	3,58858	-4,91876	-0,56133
31	6	3,9876	0,35011	4,8527
32	1	3,98501	0,83879	5,82472
33	6	5,02928	-1,12093	3,26401
34	1	5,83871	-1,79139	2,9793
35	6	3,63724	2,11958	-3,98357
36	1	3,39925	1,72958	-4,97207
37	6	2,94407	0,58564	3,97133
38	1	2,12679	1,24918	4,23849
39	6	0,34826	-3,97543	-2,40675
40	1	-0,57713	-3,70549	-2,91188
41	6	4,46177	3,22537	-3,85862
42	1	4,87332	3,7106	-4,73867
43	6	4,75918	3,70839	-2,56844
44	1	5,40767	4,57448	-2,45488
45	6	5,04737	-0,5097	4,50726
46	1	5,8624	-0,69062	5,20168
47	6	1,72988	-5,64504	-1,35375
48	1	1,90969	-6,67061	-1,04202
49	6	0,5529	-5,29786	-2,02097
50	1	-0,20448	-6,0484	-2,23257
51	26	-1,59685	-0,02744	0,03208
52	8	-1,89826	-0,20893	-1,89293
53	8	0,02228	-1,23958	0,22898
54	8	-2,90245	-1,42578	0,45793
55	7	-3,23534	1,51957	-0,07697
56	7	-1,69769	0,45207	2,20043
57	6	-1,29736	2,9696	2,15575
58	6	-3,08776	-1,47037	2,85261
59	6	-2,48153	3,31787	1,47744
60	6	-2,90661	0,02452	-2,68943
61	6	-3,38341	-1,96703	1,54187
62	6	-2,26669	-0,30641	3,08115
63	1	-2,14842	-0,0366	4,13999
64	6	-3,98255	0,89999	-2,33904
65	6	-0,9331	1,59373	2,70306
66	1	-1,01393	1,62864	3,80254
67	1	0,11783	1,40276	2,46397
68	6	-4,23736	-3,09797	1,43915
69	1	-4,46064	-3,46601	0,44186
70	6	-4,05337	1,59418	-1,0751
71	1	-4,9244	2,25726	-0,97724
72	6	-3,57314	2,32622	1,10934
73	1	-4,50067	2,88464	0,9209

74	1	-3,77534	1,63904	1,93296
75	6	0,05538	-2,37293	1,07851
76	1	-0,81095	-3,01332	0,87997
77	1	0,96722	-2,95202	0,89762
78	1	0,04226	-2,06796	2,13401
79	6	-2,67246	4,65485	1,08662
80	1	-3,58854	4,91879	0,56144
81	6	-3,98716	-0,34986	-4,85285
82	1	-3,98449	-0,8385	-5,82489
83	6	-5,02895	1,12116	-3,26421
84	1	-5,83838	1,79163	-2,97956
85	6	-3,63766	-2,11973	3,98338
86	1	-3,39979	-1,72976	4,97192
87	6	-2,94373	-0,58545	-3,97139
88	1	-2,12644	-1,24901	-4,23848
89	6	-0,34839	3,97527	2,40704
90	1	0,57696	3,70529	2,91222
91	6	-4,46219	-3,2255	3,85829
92	1	-4,87387	-3,71075	4,73827
93	6	-4,75943	-3,70848	2,56805
94	1	-5,40791	-4,57456	2,45438
95	6	-5,04693	0,50997	-4,50749
96	1	-5,86189	0,69096	-5,20198
97	6	-1,72988	5,64498	1,35403
98	1	-1,90963	6,67057	1,04233
99	6	-0,55295	5,29773	2,02132
100	1	0,20444	6,04824	2,233

**Table S6.** Optimized geometries in Cartesian coordinates for **3<sub>2</sub>-Fe<sub>2</sub>**, obtained by DFT-B3LYP calculations.

Center Number	Atomic Number	Coordinates (Angstroms)		
		X	Y	Z
1	26	-1,43626	0,64591	-0,31376
2	8	-2,32296	-0,9263	-1,08773
3	8	0,36139	0,20951	-1,18406
4	8	-3,02111	1,04265	0,77592
5	8	-3,48734	-3,31322	-1,06484
6	8	-5,48186	0,80108	2,09428
7	7	-0,79185	2,68676	0,24613
8	7	-2,3194	1,74012	-2,07217
9	6	0,55162	3,32057	-1,82567
10	6	-0,52624	3,34231	-2,73149
11	6	-3,35706	-1,09122	-1,86431
12	6	-1,36694	3,40456	1,15574
13	1	-0,88761	4,35411	1,43128
14	6	-3,3874	1,97393	1,61134
15	6	-3,86816	-0,06794	-2,71294
16	6	-4,0146	-2,36762	-1,90481
17	6	0,46038	3,20309	-0,30924
18	1	1,26484	2,54558	0,03135
19	1	0,66465	4,19535	0,12543
20	6	-2,60554	3,14664	1,85192
21	6	-4,62627	1,84987	2,31953
22	6	-3,29485	1,25667	-2,76816
23	1	-3,77904	1,9178	-3,49995
24	6	1,85522	3,46788	-2,33052
25	1	2,68816	3,42137	-1,63242
26	6	1,03309	3,68692	-4,58656

27	1	1,20473	3,83079	-5,65017
28	6	-1,97661	3,15216	-2,32166
29	1	-2,20615	3,71531	-1,41492
30	1	-2,61983	3,54988	-3,11889
31	6	-3,06069	4,13604	2,75566
32	1	-2,44624	5,01978	2,91659
33	6	-5,10077	-2,58575	-2,74132
34	1	-5,59079	-3,55332	-2,75981
35	6	0,4982	-0,13875	-2,55001
36	1	0,05378	-1,12438	-2,74594
37	1	1,55769	-0,16393	-2,82742
38	1	-0,0089	0,60079	-3,17908
39	6	-4,97615	-0,32297	-3,55899
40	1	-5,34298	0,47843	-4,19672
41	6	-0,26216	3,52343	-4,10032
42	1	-1,09925	3,53826	-4,79594
43	6	-5,58763	-1,55973	-3,57633
44	1	-6,43914	-1,75096	-4,22254
45	6	2,10274	3,65549	-3,68853
46	1	3,12414	3,76854	-4,04388
47	6	-4,26712	3,99608	3,41927
48	1	-4,61341	4,76044	4,10867
49	6	-5,04349	2,84546	3,19315
50	1	-5,99791	2,71015	3,69517
51	6	-4,06975	-4,60771	-1,06817
52	1	-5,12221	-4,57588	-0,75497
53	1	-3,49704	-5,19566	-0,34788
54	1	-3,99896	-5,07664	-2,05904
55	6	-4,98152	-0,52334	2,32292
56	1	-5,83862	-1,18655	2,18261
57	1	-4,61285	-0,61723	3,35372
58	1	-4,18764	-0,77508	1,61695
59	26	1,43621	-0,64582	0,31376
60	8	2,32293	0,92635	1,0878
61	8	-0,36142	-0,20939	1,18407
62	8	3,02106	-1,04253	-0,77592
63	8	3,48739	3,31326	1,06502
64	8	5,4818	-0,80097	-2,09428
65	7	0,79183	-2,68664	-0,24605
66	7	2,31936	-1,74014	2,0721
67	6	-0,55163	-3,32063	1,82565
68	6	0,52627	-3,34244	2,73141
69	6	3,35709	1,09119	1,86432
70	6	1,36689	-3,40442	-1,1557
71	1	0,88751	-4,35393	-1,43128
72	6	3,38736	-1,97382	-1,61131
73	6	3,86821	0,06784	2,71286
74	6	4,01467	2,36758	1,90487
75	6	-0,46042	-3,20297	0,30923
76	1	-1,26486	-2,54539	-0,03127
77	1	-0,66473	-4,19518	-0,12555
78	6	2,60549	-3,14653	-1,85188
79	6	4,62622	-1,84977	-2,31952
80	6	3,29487	-1,25674	2,76805
81	1	3,77908	-1,91793	3,49977
82	6	-1,85521	-3,46802	2,33053
83	1	-2,68818	-3,42145	1,63248
84	6	-1,03297	-3,68731	4,58651
85	1	-1,20455	-3,83131	5,65011
86	6	1,9766	-3,15222	2,3215

87	1	2,20611	-3,71528	1,4147
88	1	2,61989	-3,54998	3,11865
89	6	3,06062	-4,13592	-2,75564
90	1	2,44616	-5,01965	-2,91657
91	6	5,10091	2,58562	2,74132
92	1	5,59095	3,55317	2,75984
93	6	-0,49823	0,13885	2,55002
94	1	-0,05406	1,12461	2,7459
95	1	-1,55771	0,16376	2,8275
96	1	0,0091	-0,60054	3,17907
97	6	4,97627	0,32279	3,55884
98	1	5,34311	-0,47867	4,1965
99	6	0,26226	-3,52373	4,10022
100	1	1,09939	-3,53863	4,7958
101	6	5,58779	1,55952	3,57623
102	1	6,43936	1,75068	4,22239
103	6	-2,10265	-3,65579	3,68853
104	1	-3,12404	-3,76891	4,04392
105	6	4,26704	-3,99597	-3,41926
106	1	4,61332	-4,76033	-4,10867
107	6	5,04343	-2,84536	-3,19315
108	1	5,99784	-2,71005	-3,69518
109	6	4,06981	4,60773	1,06845
110	1	5,12226	4,57592	0,75517
111	1	3,49707	5,19577	0,34825
112	1	3,9991	5,07656	2,05937
113	6	4,98143	0,52344	-2,3229
114	1	5,83851	1,18667	-2,18259
115	1	4,61275	0,61733	-3,35371
116	1	4,18754	0,77515	-1,61693

**Table S7.** For **1-Fe<sub>2</sub>**, **2<sub>2</sub>-Fe<sub>2</sub>** and **3<sub>2</sub>-Fe<sub>2</sub>**, the general global reactivity descriptors calculated using DFT method.

Compound	Total energy, a.u.	E <sub>HOMO</sub> , a.u.	E <sub>LUMO</sub> , a.u.	Energy difference, eV	Dipole moment, D
<b>1-Fe<sub>2</sub></b>	8469.8948088294	-0,21071	-0,13229	2,13	1,40
<b>2<sub>2</sub>-Fe<sub>2</sub></b>	9584.2905735869	-0,20579	-0,10989	2,61	0,0
<b>3<sub>2</sub>-Fe<sub>2</sub></b>	12186.5635563080	-0,19818	-0,10957	2,41	0,0

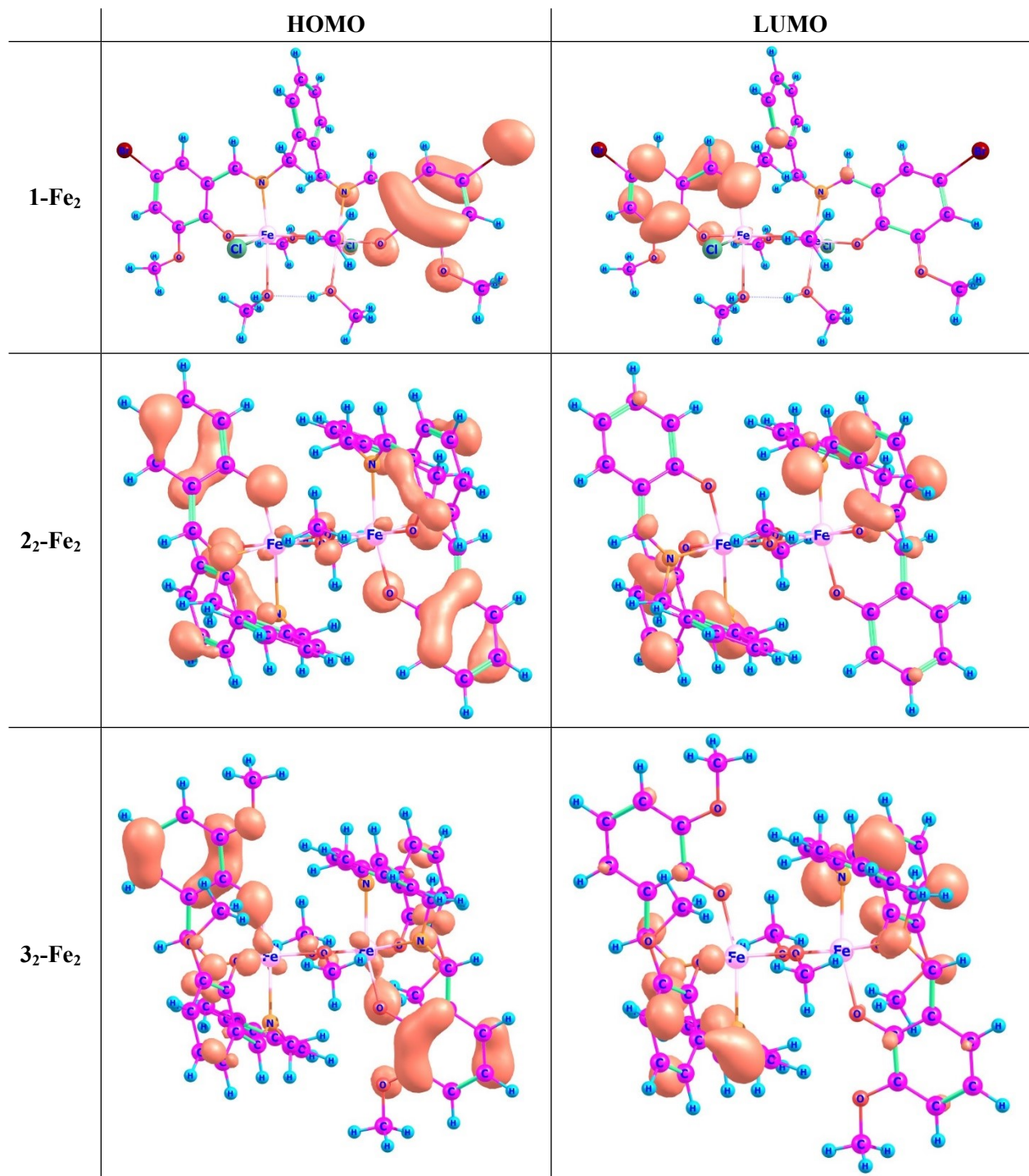


**Figure S30.** DFT- calculated HOMO/LUMO orbitals for obtained complexes. For **2<sub>2</sub>-Fe<sub>2</sub>** and **3<sub>2</sub>-Fe<sub>2</sub>**, the HOMO and LUMO orbitals are generally localized at the salicylideneamine coordinating and o-xylylene moieties, respectively. For **1-Fe<sub>2</sub>**, the HOMO and LUMO orbitals are simultaneously disposed at salicylideneamine coordinating moieties.

## 9. $^{57}\text{Fe}$ Mössbauer spectroscopy study

The  $^{57}\text{Fe}$  Mössbauer spectra were obtained on a standard MS-1104Em spectrometer no. 40-12 in the continuous acceleration mode using a symmetric sawtooth law of velocity change with separate accumulation of the spectra as the source moves forward and backward and their subsequent summation to eliminate background line distortion. A scintillation counter with a thin NaI(Tl) crystal was used as a detector. The spectra were obtained with a  $^{57}\text{Co}$  source in the Rh matrix. Calibration was performed using the  $\alpha$ -Fe spectrum, and isomer shifts were measured from the “center of gravity” of the spectrum obtained at room temperature (RT) of this reference. Mathematical handling of the gained spectra was carried out through the standard Mössbauer program UnivemMS. All samples were placed in aluminum holder which was attached to the liquid nitrogen cryostat and their temperature was being changed between 79 – 300 K by temperature controller with accuracy  $\pm 0.5$  K.

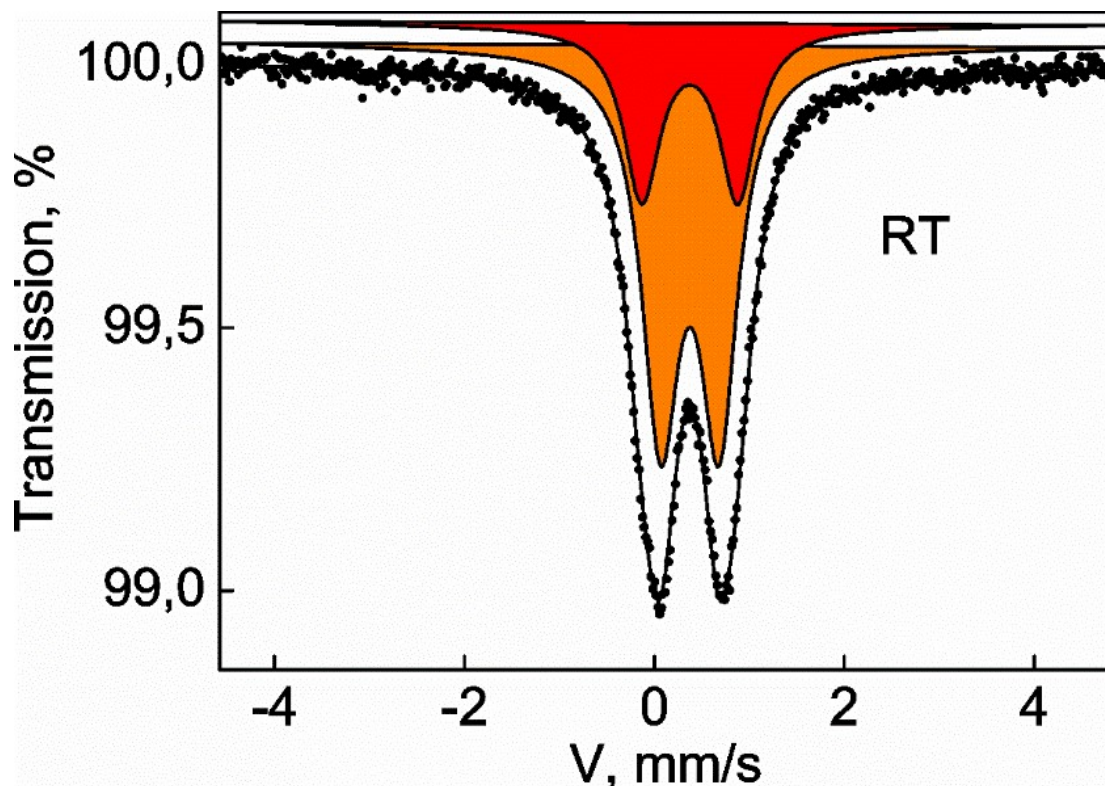


**Figure S31.**  $^{57}\text{Fe}$  Mössbauer spectra scaled to the same Doppler velocity area of as prepared powdered sample of  $\mathbf{2}_2\text{-Fe}_2$  measured at room temperature (**solid circles**). Best fit lines for Mössbauer spectra and quadrupole hyperfine doublets – **solid lines**. HS components - **red** and **orange** areas.

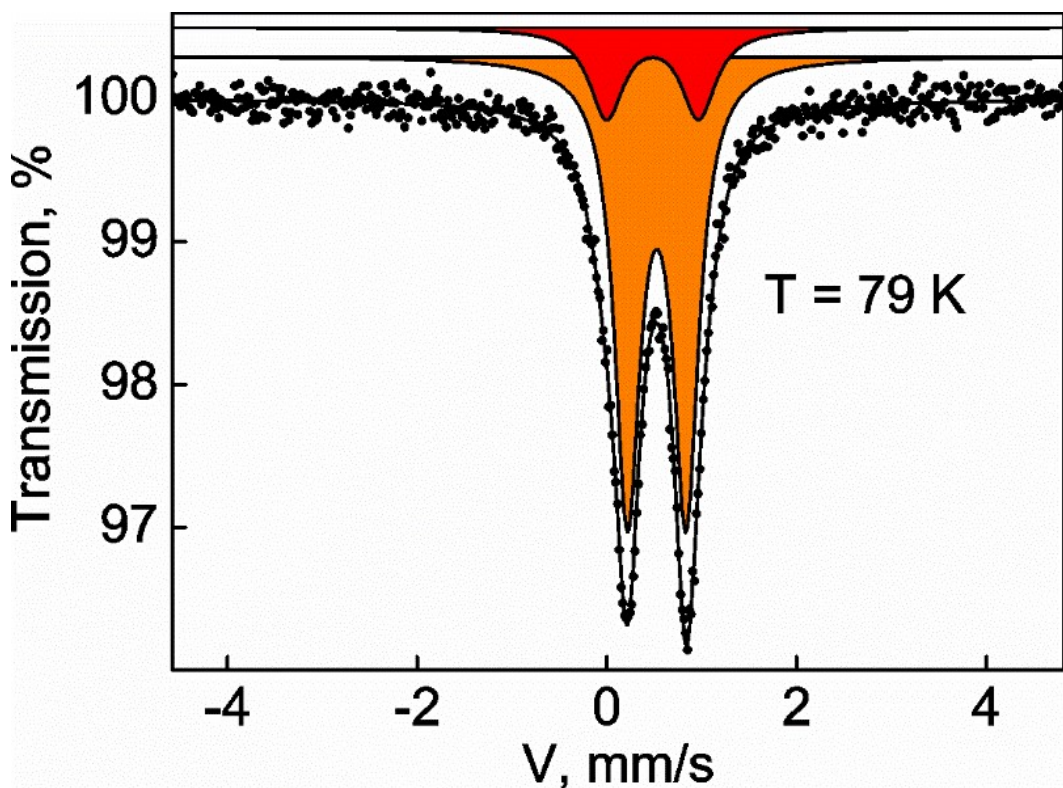


**Figure 32.**  $^{57}\text{Fe}$  Mössbauer spectra scaled to the same Doppler velocity area of as prepared powdered sample of  $\mathbf{2_2\text{-Fe}_2}$ , measured at 79 K (solid circles). Best fit lines for Mössbauer spectra and quadrupole hyperfine doublets – solid lines. HS components - red and orange areas.

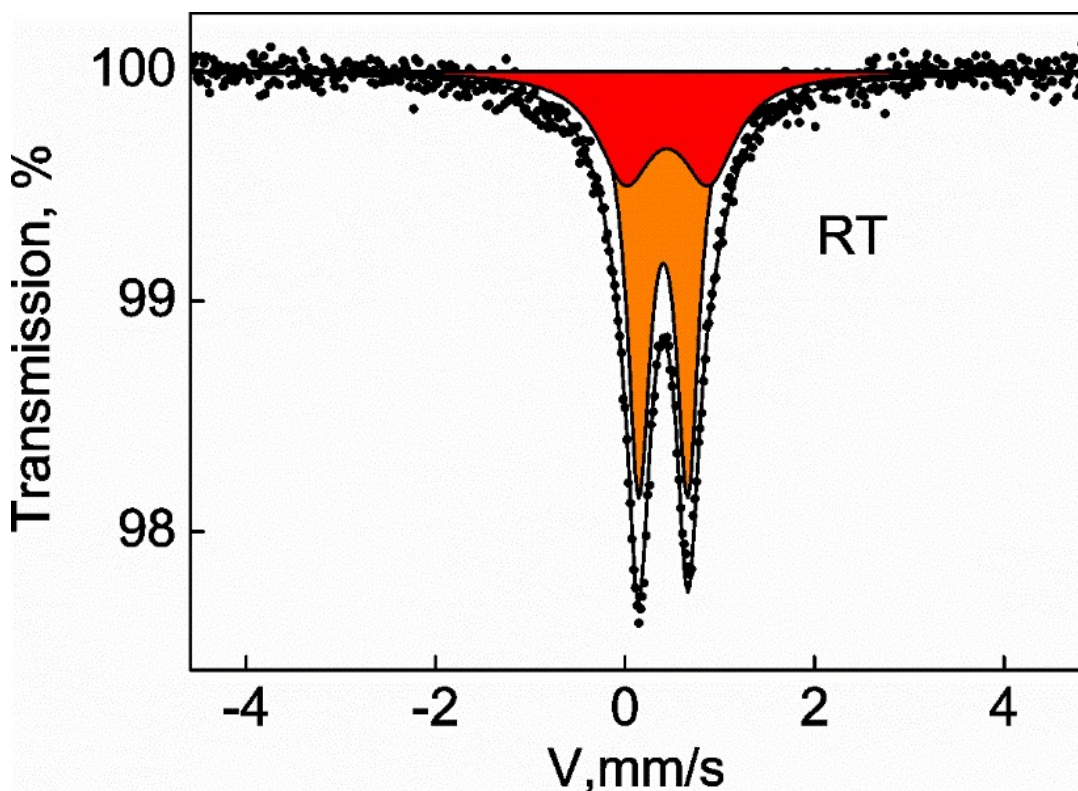


**Figure 33.**  $^{57}\text{Fe}$  Mössbauer spectra scaled to the same Doppler velocity area of as prepared powdered sample of  $\mathbf{3_2\text{-Fe}_2}$ , measured at room temperature (solid circles). Best fit lines for Mössbauer spectra and quadrupole hyperfine doublets – solid lines. HS components - red and orange areas.

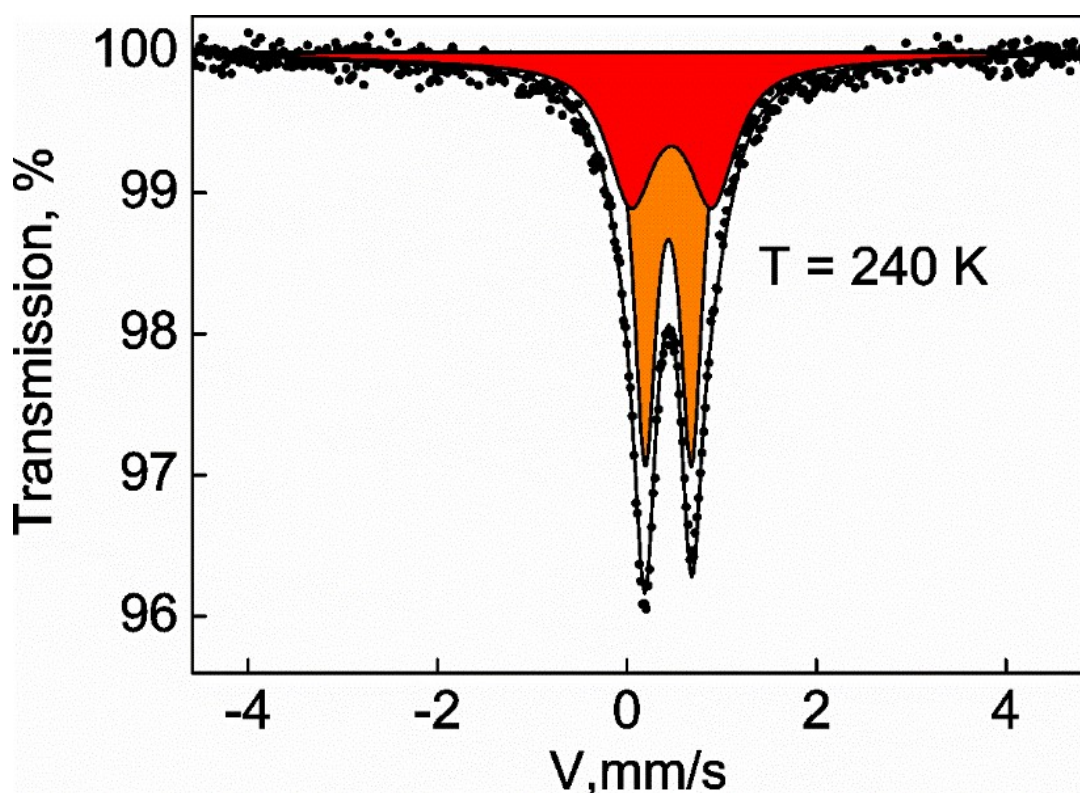


**Figure S34.**  $^{57}\text{Fe}$  Mössbauer spectra scaled to the same Doppler velocity area of as prepared powdered sample of  $\mathbf{3}_2\text{-Fe}_2$ , measured at 240 K (solid circles). Best fit lines for Mössbauer spectra and quadrupole hyperfine doublets – solid lines. HS components – red and orange areas.

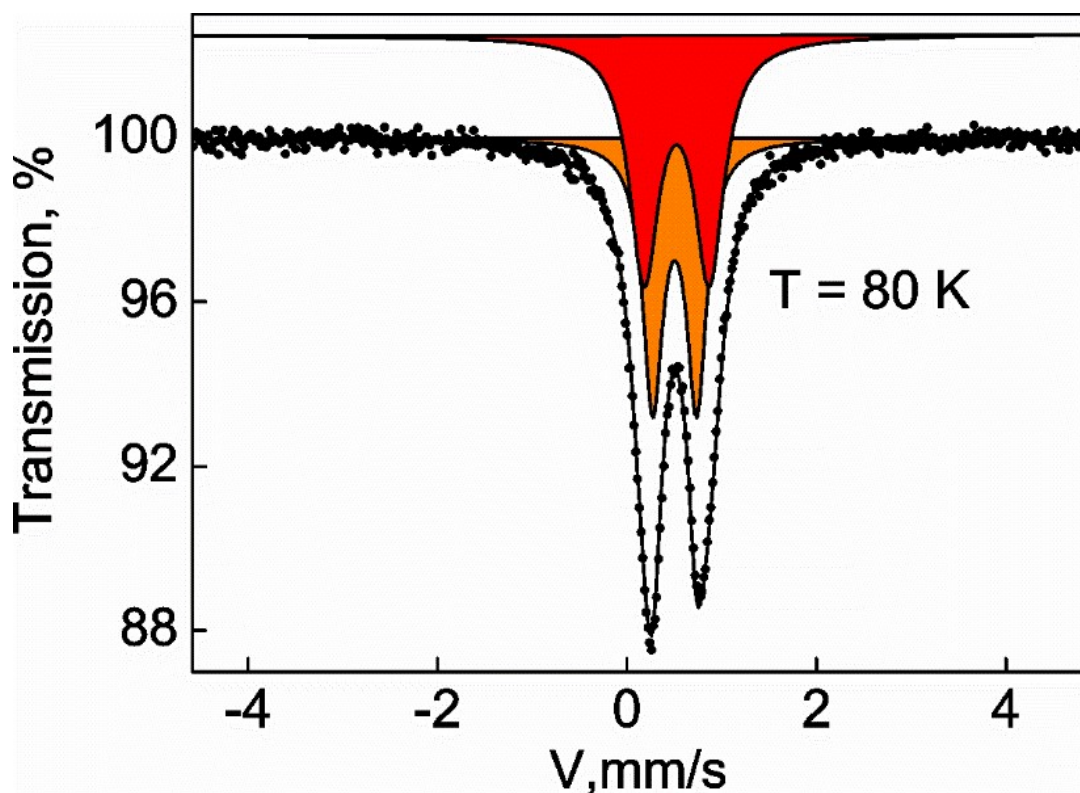


**Figure S35.**  $^{57}\text{Fe}$  Mössbauer spectra scaled to the same Doppler velocity area of as prepared powdered sample of  $\mathbf{3}_2\text{-Fe}_2$ , measured at 80 K (solid circles). Best fit lines for Mössbauer spectra and quadrupole hyperfine doublets – solid lines. HS components – red and orange areas.



**Table S8.** The parameters of  $^{57}\text{Fe}$  Mössbauer spectra for **1-Fe<sub>2</sub>**, **2<sub>2</sub>-Fe<sub>2</sub>** and **3<sub>2</sub>-Fe<sub>2</sub>** obtained at different temperature.

Compound	Signal	T, $\pm 0.5$ K	$\delta_{\text{Fe}}$ , $\pm 0.01$ mm·s <sup>-1</sup>	$\Delta E_Q$ , $\pm 0.01$ mm·s <sup>-1</sup>	$\Gamma$ , $\pm 0.01$ mm·s <sup>-1</sup>	RA, $\pm 1$ %	Spin State
1-Fe <sub>2</sub>	D1	RT	<b>0.42</b>	<b>1.21</b>	<b>0.39</b>	<b>46.8</b>	<b>HS<sub>1</sub></b>
	D2		<b>0.38</b>	<b>0.60</b>	<b>0.36</b>	<b>53.2</b>	<b>HS<sub>2</sub></b>
	D1	240	<b>0.46</b>	<b>1.22</b>	<b>0.34</b>	<b>47.1</b>	<b>HS<sub>1</sub></b>
	D2		<b>0.42</b>	<b>0.64</b>	<b>0.36</b>	<b>52.9</b>	<b>HS<sub>2</sub></b>
	D1	80	<b>0.53</b>	<b>1.24</b>	<b>0.26</b>	<b>50.4</b>	<b>HS<sub>1</sub></b>
	D2		<b>0.54</b>	<b>0.81</b>	<b>0.54</b>	<b>49.6</b>	<b>HS<sub>2</sub></b>
2 <sub>2</sub> -Fe <sub>2</sub>	D1	RT	<b>0.37</b>	<b>1.01</b>	<b>0.48</b>	<b>30.7</b>	<b>HS<sub>1</sub></b>
	D2		<b>0.35</b>	<b>0.61</b>	<b>0.46</b>	<b>69.3</b>	<b>HS<sub>2</sub></b>
	D1	79	<b>0.48</b>	<b>0.97</b>	<b>0.44</b>	<b>20.9</b>	<b>HS<sub>1</sub></b>
	D2		<b>0.52</b>	<b>0.62</b>	<b>0.32</b>	<b>79.1</b>	<b>HS<sub>2</sub></b>
3 <sub>2</sub> -Fe <sub>2</sub>	D1	RT	<b>0.44</b>	<b>0.88</b>	<b>0.69</b>	<b>37.1</b>	<b>HS<sub>1</sub></b>
	D2		<b>0.40</b>	<b>0.52</b>	<b>0.29</b>	<b>62.9</b>	<b>HS<sub>2</sub></b>
	D1	240	<b>0.47</b>	<b>0.86</b>	<b>0.59</b>	<b>42.4</b>	<b>HS<sub>1</sub></b>
	D2		<b>0.44</b>	<b>0.49</b>	<b>0.28</b>	<b>57.6</b>	<b>HS<sub>2</sub></b>
	D1	80	<b>0.52</b>	<b>0.69</b>	<b>0.38</b>	<b>56.9</b>	<b>HS<sub>1</sub></b>
	D2		<b>0.50</b>	<b>0.46</b>	<b>0.26</b>	<b>43.1</b>	<b>HS<sub>2</sub></b>

$\delta_{\text{Fe}}$  - isomer shift (with reference to metallic iron at RT),

$\Delta E_Q$  - quadrupole splitting,

$\Gamma$  - half-height width,

RA - relative area.

- 
- 1 *ORGANIKUM. Organisch-chemisches Grundpraktikum*, H. G. Becker, W. Berger, G. Domschke, Deutscher Verlag der Wissenschaften, Berlin, 1965.
  - 2 L. Krause, R. Herbst-Irmer, G. M. Sheldrick, D. Stalke, Comparison of silver and molybdenum microfocus X-ray sources for single-crystal structure determination, *J. Appl. Crystallogr.*, **2015**, *48*, 3–10. DOI: 10.1107/S1600576714022985
  - 3 O. V. Dolomanov, L. J. Bourhis, R. J. Gildea, J. A. K. Howard, H. Puschmann, *OLEX2: A Complete Structure Solution, Refinement and Analysis Program*, *J. Appl. Crystallogr.*, **2009**, *42*, 339–341. DOI: 10.1107/S0021889808042726
  - 4 G. M. Sheldrick, *SHELXT – Integrated space-group and crystal-structure determination*, *Acta Crystallogr., Sect. A: Found. Adv.*, **2015**, *71*, 3–8. DOI: 10.1107/S2053273314026370
  - 5 G. M. Sheldrick, *SHELXT – Integrated space-group and crystal-structure determination*, *Acta Crystallogr., Sect. A: Found. Adv.*, **2015**, *71*, 3–8. DOI: 10.1107/S2053273314026370
  - 6 L. J. Farrugia, *WinGX* and *ORTEP* for *Windows*: an update, *J. Appl. Crystallogr.* **2012**, *45*, 849–854. DOI: 10.1107/S0021889812029111
  - 7 R. Ketkaew, Y. Tantirungrotechai, P. Harding, G. Chastanet, P. Guionneau, M. Marchivie, D. J. Harding, OctaDist: a tool for calculating distortion parameters in spin crossover and coordination complexes, *Dalton Trans.*, **2021**, *50*, 3, 1086. DOI: 10.1039/D0DT03988H
  - 8 M. J. Frisch, G. W. Trucks, H. B. Schlegel, G. E. Scuseria, M. A. Robb, J. R. Cheeseman, G. Scalmani, V. Barone, B. Mennucci, G. A. Petersson, H. Nakatsuji, M. Caricato, X. Li, H. P. Hratchian, A. F. Izmaylov, J. Bloino, G. Zheng, J. L. Sonnenberg, M. Hada, M. Ehara, K. Toyota, R. Fukuda, J. Hasegawa, M. Ishida, T. Nakajima, Y. Honda, O. Kitao, H. Nakai, T. Vreven, J. A. Montgomery Jr., J. E. Peralta, F. Ogliaro, M. Bearpark, J. J. Heyd, E. Brothers, K. N. Kudin, V. N. Staroverov, R. Kobayashi, J. Normand, K. Raghavachari, A. Rendell, J. C. Burant, S. S. Iyengar, J. Tomasi, M. Cossi, N. Rega, J. M. Millam, M. Klene, J. E. Knox, J. B. Cross, V. Bakken, C. Adamo, J. Jaramillo, R. Gomperts, R. E. Stratmann, O. Yazyev, A. J. Austin, R. Cammi, C. Pomelli, J. W. Ochterski, R. L. Martin, K. Morokuma, V. G. Zakrzewski, G. A. Voth, P. Salvador, J. J. Dannenberg, S. Dapprich, A. D. Daniels, O. Farkas, J. B. Foresman, J. V. Ortiz, J. Cioslowski, D. J. Fox, *Gaussian 09, Revision E.01*, Inc Wallingford, CT, 2009.
  - 9 A. D. Becke, Density-functional thermochemistry. III. The role of exact exchange, *J. Chem. Phys.*, **1993**, *98*, 5648. DOI: 10.1063/1.464913
  - 10 C. Lee, W. Yang, R.G. Parr, Development of the Colle-Salvetti correlation-energy formula into a functional of the electron density, *Phys. Rev. B*, **1988**, *37*, 785. DOI: 10.1103/PhysRevB.37.785.